Human Molecular Genetics, 2021, Vol. 30, No. 17 1649–1665

https://doi.org/10.1093/hmg/ddab155
Advance Access Publication Date: 7 June 2021
General Article

GENERAL ARTICLE

Identification of the GlialCAM interactome: the G protein-coupled receptors GPRC5B and GPR37L1 modulate megalencephalic leukoencephalopathy proteins

Marta Alonso-Gardón[1,2,#], Xabier Elorza-Vidal[1,2,#], Aida Castellanos[1,2], Gina La Sala[3], Mercedes Armand-Ugon[1], Alice Gilbert[4], Chiara Di Pietro[3], Adrià Pla-Casillanis[1], Francisco Ciruela[5], Xavier Gasull[6], Virginia Nunes[7], Albert Martínez[8], Uwe Schulte[9], Martine Cohen-Salmon[4], Daniela Marazziti[3] and Raúl Estévez[1,2,*,†]

[1]Departament de Ciències Fisiològiques, Genes Disease and Therapy Program IDIBELL - Institute of Neurosciences, Universitat de Barcelona, Barcelona 08036, Spain, [2]Centro de Investigación Biomédica en Red sobre Enfermedades Raras (CIBERER), Instituto de Salud Carlos III, Madrid 28029, Spain, [3]Institute of Biochemistry and Cell Biology, Italian National Research Council (CNR), Monterotondo Scalo, Rome I-00015, Italy, [4]Physiology and Physiopathology of the Gliovascular Unit Research Group, Center for Interdisciplinary Research in Biology (CIRB), College de France, CNRS Unité Mixte de Recherche 724, INSERM Unité 1050, Labex Memolife, PSL Research University, Paris F-75005, France, [5]Pharmacology Unit, Department of Pathology and Experimental Therapeutics, Faculty of Medicine and Health Sciences, Institute of Neurosciences, University of Barcelona-IDIBELL, L'Hospitalet de Llobregat, Barcelona 08036, Spain, [6]Neurophysiology Laboratory, Department of Biomedicine, Medical School, Institute of Neurosciences, University of Barcelona-IDIBAPS, Casanova 143 Barcelona 08036, Spain, [7]Unitat de Genètica, Departament de Ciències Fisiològiques, Universitat de Barcelona, Laboratori de Genètica Molecular, Genes Disease and Therapy Program IDIBELL, L'Hospitalet de Llobregat 08036, Spain, [8]Department of Cell Biology, Physiology and Immunology, Faculty of Biology, University of Barcelona, Barcelona 08028, Spain and [9]Logopharm GmbH, Freiburg 79104, Germany

*To whom correspondence should be addressed at: Facultat de Medicina, Departament de Ciències Fisiològiques, Universitat de Barcelona-IDIBELL, C/Feixa Llarga s/n 08907 L'Hospitalet de Llobregat, Barcelona 08028, Spain. Tel: +34 934039781; Fax: +34 934024268; Email: restevez@ub.edu

Abstract

Megalencephalic Leukoencephalopathy with subcortical Cysts (MLC) is a type of vacuolating leukodystrophy, which is mainly caused by mutations in *MLC1* or *GLIALCAM*. The two MLC-causing genes encode for membrane proteins of yet unknown function that have been linked to the regulation of different chloride channels such as the ClC-2 and VRAC. To gain insight into the role of MLC proteins, we have determined the brain GlialCAM interacting proteome. The proteome

†Raúl Estévez, http://orcid.org/0000-0003-1579-650X
#These two authors contributed equally to this study and share first authorship.

Received: March 31, 2021. **Revised:** May 31, 2021. **Accepted:** June 1, 2021

includes different transporters and ion channels known to be involved in the regulation of brain homeostasis, proteins related to adhesion or signaling as several G protein-coupled receptors (GPCRs), including the orphan GPRC5B and the proposed prosaposin receptor GPR37L1. Focusing on these two GPCRs, we could validate that they interact directly with MLC proteins. The inactivation of *Gpr37l1* in mice upregulated MLC proteins without altering their localization. Conversely, a reduction of GPRC5B levels in primary astrocytes downregulated MLC proteins, leading to an impaired activation of ClC-2 and VRAC. The interaction between the GPCRs and MLC1 was dynamically regulated upon changes in the osmolarity or potassium concentration. We propose that GlialCAM and MLC1 associate with different integral membrane proteins modulating their functions and acting as a recruitment site for various signaling components as the GPCRs identified here. We hypothesized that the GlialCAM/MLC1 complex is working as an adhesion molecule coupled to a tetraspanin-like molecule performing regulatory effects through direct binding or influencing signal transduction events.

Introduction

Megalencephalic Leukoencephalopathy with subcortical Cysts (MLC) is a rare type of leukodystrophy (1). Patients suffering from MLC present macrocephaly, subcortical cysts and white matter vacuolation, leading to epilepsy as well as motor and cognitive impairments (2). MLC is caused by mutations in either *MLC1* (3) or *GLIALCAM* (also called *HEPACAM*) (4). These genes encode for membrane proteins that form a complex located at cell–cell junctions in brain perivascular astrocytic processes or in Bergmann glia at the cerebellum (5). A reduced number of patients (2%) do not harbor mutations in *MLC1* or *GLIALCAM*, suggesting the existence of other unknown disease genes (6).

The functional role of the GlialCAM/MLC1 complex is still unknown. Nevertheless, different proteins and activities related to brain homeostasis are affected in a GlialCAM or MLC1-dependent manner. Therefore, a role for these proteins in neuronal ion/water homeostasis has been hypothesized. For instance, depletion of MLC1 has been shown to reduce VRAC activity in primary astrocytes (7,8). In addition, GlialCAM and MLC1 have been shown to form a ternary complex with the ClC-2 chloride channel (9). Also, co-expression of human GlialCAM with ClC-2 changes the channel activity from inwardly rectifying to an ohmic channel (10). Furthermore, the Na^+/K^+-ATPase pump has been identified as a MLC1-interacting protein, whereas the overexpression of MLC1 was observed to reduce its activity (11). Finally, Cx43 has been identified as a GlialCAM interacting protein (12) and MLC1 might influence Cx43 stability at gap junctions in astrocytoma cells (13).

It is not clear how GlialCAM and MLC1 affect the activity of different ion channels and transporters. It has been suggested that they might influence signaling cascades by yet undefined mechanisms (14). In this sense, recent work has shown that the overexpression of human MLC1 in astrocytes decreases the phosphorylation of extracellular signal-regulated kinases (ERK), whereas primary astrocytes lacking MLC1 show an increase in ERK phosphorylation (15).

In summary, although it is clear that GlialCAM/MLC1 proteins regulate the activity of different ion channels and transporters that play a role in neuronal brain homeostasis, the mechanisms involved in this process remain unclear. Here, we have determined the GlialCAM interactome from mouse brain and analyzed its interaction with GlialCAM and MLC1. Among the proteins identified as part of this network, we found specific G protein-coupled receptors (GPCRs), concretely the orphan GPRC5B (16) and the proposed prosaposin receptor GPR37L1 (17), which show a dynamic association with GlialCAM and MLC1 and regulate their surface levels. Based on the results of this work, we propose a functional role for GlialCAM and MLC1 proteins.

Results

Identification of the GlialCAM interactome

For comprehensive identification of the GlialCAM interactome, we performed affinity purifications (APs) with four different antibodies specific for GlialCAM on membrane fractions prepared from whole brains from adult rats, wild-type (WT) mice, and *Glialcam* knockout (KO) mice (10). Membranes were solubilized with the detergent buffer CL-47 plus 1 mM Mg^{2+}, as earlier experiments indicated that this detergent mixture was able to maintain the interaction of GlialCAM with MLC1 and ClC-2, two previously validated interactors (4,9). Total eluates of APs with the anti-GlialCAM antibodies or with unspecific immunoglobulins G (IgG) were analyzed by high-resolution nanoflow liquid chromatography-tandem mass spectrometry (LC-MS/MS), which provided data on both the identity and the amount of interacting proteins. Two out of the four anti-GlialCAM antibodies purified their target with high efficiency, allowing for a more detailed analysis of the main target's primary sequence. MS analyses showed that GlialCAM, MLC1 and ClC-2 proteins were retained in all APs with high efficiency, as reflected by the peak volume (PV) values (see Materials and Methods) and the extensive coverage of protein sequences (relative sequence coverage of 72, 53 and 74%, respectively). The other proteins identified by MS were evaluated for both their specifity and consistency of copurification with the GlialCAM protein based on the quantitative data of protein amounts. For each protein, the consistency of enrichment was evaluated with the different antibodies and its quantitative correlation with the purified GlialCAM protein.

Together, these criteria defined a sharp-profiled proteome (Fig. 1A for one GlialCAM antibody and Supplementary Material, Fig. S1 for another GlialCAM antibody), identifying 21 proteins as high-confidence constituents of the GlialCAM interactome in the mouse brain. As summarized in (Fig. 1B), these constituents comprise the aforementioned GlialCAM, MLC1 and ClC-2 and previously identified transport/ion channels proteins interacting with GlialCAM or MLC1. These include the gap junction protein Cx43 (12,13), the glutamate transporters EAAT1/2 and the sodium/potassium ATPase subunits alpha2 and beta2 (11,18). Other proteins that mediate transport or have been related to chloride channel function such as the bicarbonate transporter (NBCe1), the glucose transporter (GLUT1), the sodium/calcium exchanger 1 (NCX1) or the protein tweety-homolog 1 were also identified. In previous APs experiments using MLC1 antibodies, NBCe1 and tweety-homolog 1 were also specifically co-purified with MLC1 (Fig. 1B).

Apart from transporters and ion channels, we identified proteins related to cell adhesion or trafficking such as tetraspanin-9 (CD9), Neuronal membrane glycoprotein M6-a/b (GPM6A/B) or Syntaxin-1A/1B. Interestingly, CD9 was also identified in a membrane yeast two-hybrid (MYTH) screening using human

A

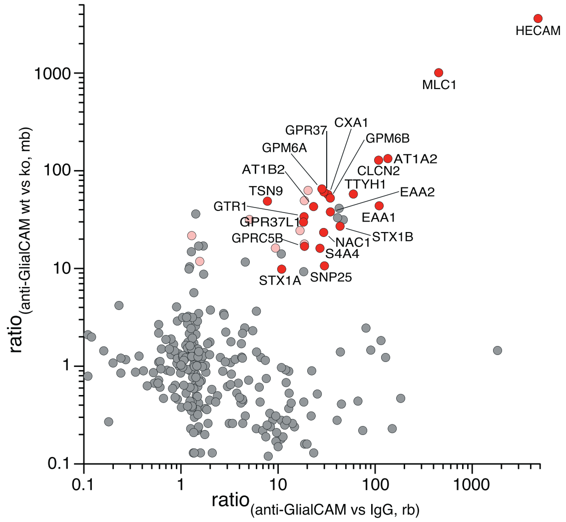

B

Identified proteins	MLC1 IP
HECAM: Hepatocyte cell adhesion molecule	yes
MLC1: Membrane protein MLC1	yes
Transport/Ion channels	
CLCN2: Chloride channel protein 2 (Clc-2)	yes
CXA1: Connexin 43	no
EAA1: Excitatory amino acid transporter 1 (Glast)	yes
EAA2: Excitatory amino acid transporter 2 (Glt-1)	yes
AT1A2: Sodium/potassium-transporting ATPase subunit alpha-2	yes
S4A4: Electrogenic sodium bicarbonate cotransporter 1 (Nbce1)	yes
TTYH1: Protein tweety homolog1	yes
AT1B2: Sodium/potassium-transporting ATPase subunit beta-2	yes
GTR1: Solute carrier family 2, facilitated glucose transporter member 1 (Glut1)	no
NAC1: Sodium/calcium exchanger 1 (Ncx1)	no
Signalling	
GPR37: Prosaposin receptor GPR37	no
GPR37L1: G-protein coupled receptor 37-like 1	no
GPRC5B: G-protein coupled receptor family C group 5 member B	yes*
Adhesion/Junctions/Trafficking	
TSN9: Tetraspanin-9 (CD9)	no*
GPM6A: Neuronal membrane glycoprotein M6-a	yes
GPM6B: Neuronal membrane glycoprotein M6-b	yes
STX1B: Syntaxin-1B	no
STX1A: Syntaxin-1A	no
SNP25: Synaptosomal-associated protein 25	no

* Identified in MYTH screenings using human MLC1 as bait.

Figure 1. Identification of the GlialCAM interactome. (**A**) Specificity map of the GlialCAM interactome with one of the rabbit polyclonal anti-GlialCAM antibodies used that detects a peptide from the C-terminus. Two-dimensional logarithmic abundance-ratio plot illustrating the medians of PV ratios (rPV) obtained for any protein in APs from rat membranes with the *second* anti-GlialCAM antibody used versus IgG (x axis) and in anti-glialCAM APs from mouse membranes of wild-type (WT) versus *Glialcam* KO animals (y axis). Gray bars (rPVs of 10) represent the specificity threshold for this AB on either rPV scale and place specifically purified proteins in the upper-right quadrant. Red dots denote finally annotated GlialCAM constituents (**B**); black dots symbolize all other proteins. (B) List of proteins belonging to the GlialCAM interactome classified according to their assigned function. We indicate if they have been identified in AP using anti MLC1 antibodies and in MYTH screening using human MLC1 as a bait.

MLC1 as a bait, indicating direct interaction. GPM6A/B were also identified in MLC1 APs (Fig. 1B).

Finally, three GPCRs were identified as components of the GlialCAM interactome. One of these, the orphan GPRC5B (also named RAIG2) was also identified in a MYTH using human MLC1 as a bait and also in APs using MLC1 antibodies. Therefore, it can be considered a bona fide interactor. Interestingly, the two other identified GPCRs (GPR37 and GPR37l1) belong to the same protein family (19).

Interactions between GPCRs and GlialCAM/MLC1

GlialCAM and MLC1 have been related to signal transduction changes, but the mechanisms involved in this process remain unresolved (14,15). In this regard, we considered the identified GPCRs as candidates for the signal transduction changes related to GlialCAM/MLC1 and proceeded to characterize their interaction with MLC proteins. As MLC1 is only astrocytic (20), we focused on GPRC5B and GPR37L1 and not on GPR37, which is mainly expressed in oligodendrocytes (21).

We developed a polyclonal antibody which was able to detect specifically GPRC5B by Western blot (Supplementary Material, Fig. S2A–B) and by immunofluorescence on primary astrocytes (Supplementary Material, Fig. S2C). The antibody was validated in siRNA and overexpression experiments. For GPR37L1, we used commercially available antibodies (see Materials and Methods) previously validated using *Gpr37l1* KO animals (22).

Co-localization was tested and observed between MLC1 and GPRC5B (Fig. 2A) or GPR37L1 (Fig. 2B) in primary cultures of astrocytes. We assessed colocalization with MLC1 and not with GlialCAM, as both proteins colocalize perfectly in astrocytes and we have anti-MLC1 polyclonal and monoclonal antibodies directed against the same MLC1 intracellular epitopes (23) and therefore, are suitable for all experiments.

Proximity-ligation assays (PLA) in primary cultures revealed close proximity between GPRC5B or GPR37L1 and MLC1 (Fig. 2C and D). Control experiments in WT cells without the primary antibody or in astrocytes obtained from *Mlc1* KO animals (10) demonstrated the specificity of the PLA signal (Fig. 2C and D).

At a tissular level, we could not detect a specific signal for GPRC5B with the new antibody or with commercially available ones. However, in purified gliovascular units (GVUs), a preparation more accessible to detect astrocytic endfeet proteins (24), we could detect partial co-localization between GPRC5B and MLC1 (Fig. 3A). GPR37L1 is mainly expressed in Bergmann glia (25), where GlialCAM and MLC1 are also expressed. However, co-localization between GPR37L1 and MLC1 in Bergmann glia (Fig. 3B) was low. The fact that the co-localization between the GPCRs and MLC1 was higher in primary cultures could indicate that the accessibility of the antibodies against the GPCRs might be limited in brain tissue preparations.

The ability of human GPRC5B or GPR37L1 to physically interact in living cells with human GlialCAM or MLC1 was then assessed *in vitro* by means of bioluminescence resonance energy transfer (BRET) saturation assays. HEK293T cells were co-transfected with a constant amount of either the GPRC5B-Rluc or the GPR37L1-Rluc plasmids combined with increasing concentrations of the MLC1-VFP (Fig. 4A) or GlialCAM-VFP (Fig. 4B) plasmids. The interaction between GlialCAM and MLC1 (Fig. 4A) was used as positive control, whereas the lack of interaction between LRRC8A [the main subunit of the VRAC channel (26,27)] and either MLC1 (Fig. 4A) or GlialCAM (Fig. 4B) was used as a negative control. A positive BRET signal was detected when GPRC5B or GPR37L1 were co-expressed with MLC1 (Fig. 4A) or with GlialCAM (Fig. 4B). The determination of the $BRET_{50}$ signal allowed to compare the strength of interaction between GPR37L1 or GPRC5B with MLC1 versus the interaction with GlialCAM. The $BRET_{50}$ values for the interaction of GPR37L1 with MLC1 and GPR37L1 with GlialCAM were 2.9 ± 0.9 ($n = 5$) and 2.6 ± 0.4 ($n = 4$), respectively, which were not statistically different ($P = 0.73$). Similarly, the $BRET_{50}$ values for the interaction of GPRC5B with MLC1 and GPRC5B with GlialCAM were 1.2 ± 0.3 ($n = 4$) and 0.7 ± 0.2 ($n = 5$), which were also not statistically different ($P = 0.19$), indicating that GPCRs interact with MLC1 and GlialCAM with similar avidity.

These results demonstrated that GPRC5B or GPR37L1 and the MLC proteins are in close proximity (<10 nm). Together with

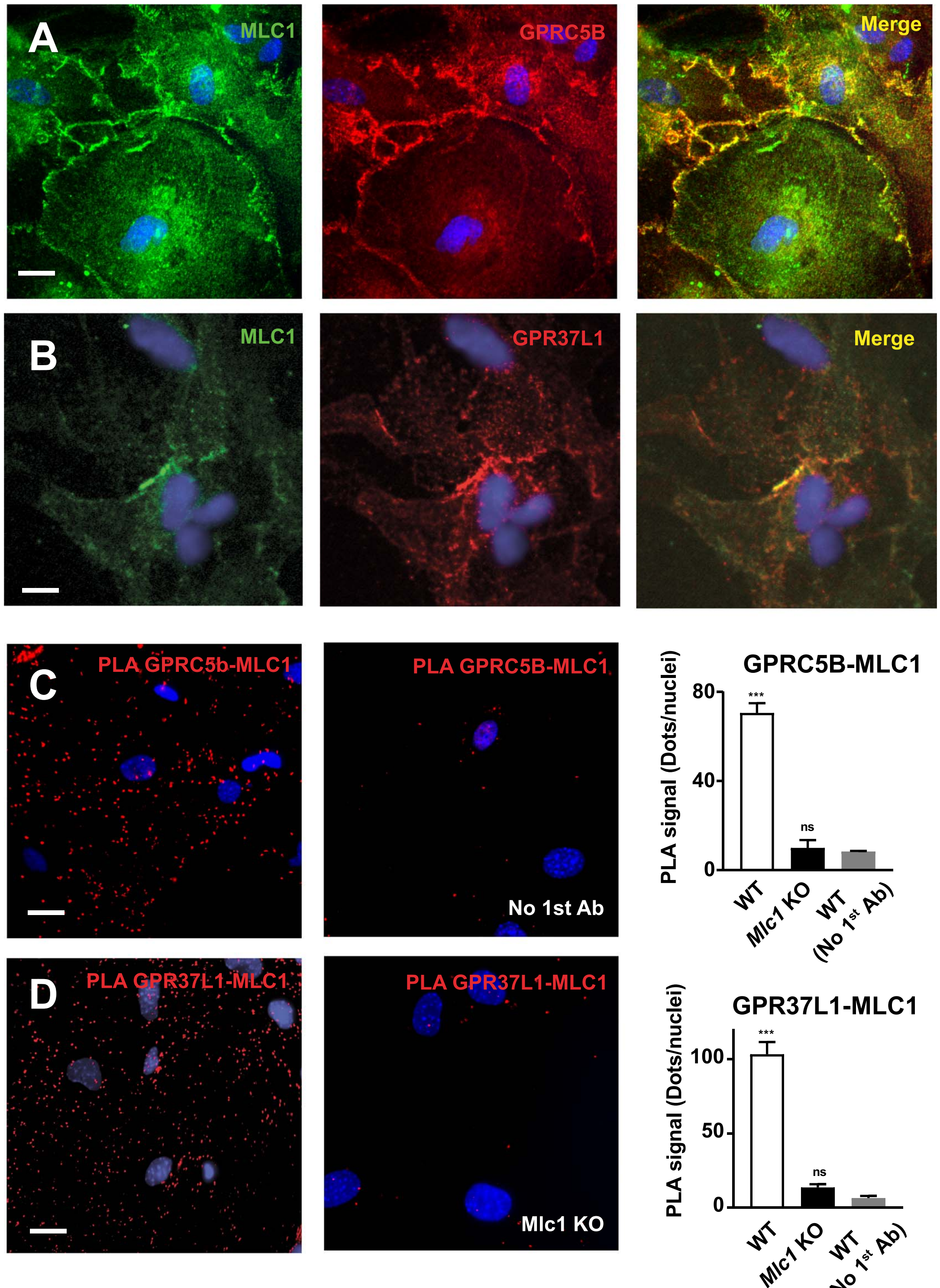

Figure 2. Localization of GPRC5B and GPR37L1 in primary cultures of astrocytes. (**A**) Representative images of immunostaining of MLC1 in green (left), GPRC5B in red (middle) and merged stainings where the two proteins show a certain degree of colocalization at the plasma membrane (right, yellow) from cultured mouse astrocytes. Scale bar, 20 μm (**B**) Representative confocal images of MLC1 (green), GPR37L1 (red), co-immunofluorescence labeling and DAPI staining (blue) in mouse cerebellar primary astrocytes from wild-type (WT) pups. Scale bar, 75 μm. (**C** and **D**) PLA for protein interactions between MLC1 and GPRC5B (C) or GPR37L1 (D) in WT or *Mlc1* KO cultured mouse astrocytes. Cells with only one primary antibody (MLC1 antibody) were used as negative controls. Scale bar, 20 μm. The number of PLA dots was quantified using Image J. Data are mean ± standard error of the mean of three–four independent experiments. For statistical analyses, we performed a one-way analysis of variance plus Dunnet multiple comparison's test versus the negative control. ns, not significant. $^{***}P < 0.001$.

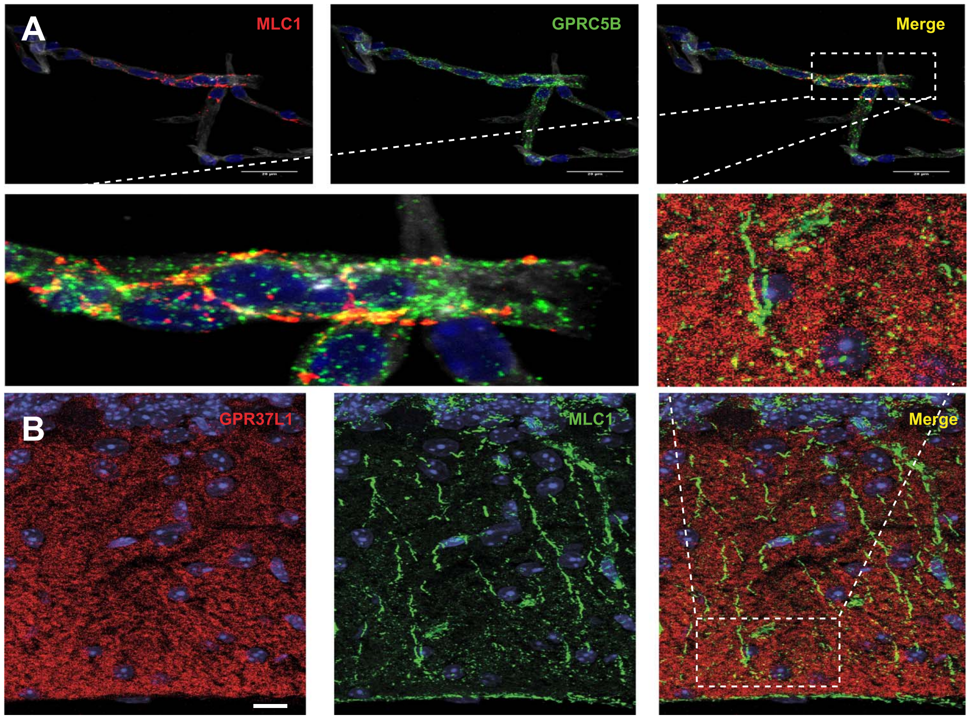

Figure 3. Localization of the identified GPCRs with MLC1 in brain slices. (**A**) The localization of GPRC5B and MLC1 in GVUs. Projection confocal plan of MLC1 (red) and GPRC5B (green) immunolabeled GVUs purified from adult wild-type (WT) brain. Nuclei are labeled with Hoechst (blue) and blood vessel wall with Isolectin B4 (white). Scale bar, 20 μm. (**B**) The localization of GPR37L1 and MLC1 in Bergmann glia. Representative confocal images of GPR37L1 (red), MLC1 (green) co-immunofluorescence labeling and DAPI staining (blue), in cerebellar coronal sections of WT adult mice. Higher magnifications of boxed areas (dashed lines) in (A) and (B) are presented. Scale bar, 20 μm.

our data obtained from slices and cell culture, they support the existence of GPCRs-MLC protein complexes in living cells.

Lack of GPR37L1 increases MLC proteins in vivo

GPR37L1 is expressed exclusively in astrocytes and immature oligodendrocytes within the brain, also being highly expressed in Bergmann glia of the cerebellum (25). *Gpr37l1* KO mice showed no alteration of adult cerebellar layer cytoanatomy and organization and no signs of gliosis. At the functional level, animals presented improved motor functions and advanced cerebellar development (22). Based on the similarities of expression patterns for GlialCAM, MLC1 and GPR37L1 together with the mild phenotype of the KO mice, we reasoned that the analysis of MLC proteins in *Gpr37l1* KO mice may suggest direct effects of GPR37L1 in MLC protein biology.

We first analyzed the consequences of the lack of GPR37L1 on MLC1 and GlialCAM protein levels. Western blot experiments of cerebellum membranes indicated that both proteins were upregulated in the *Gpr37l1* KO (Fig. 5A). Because GlialCAM and MLC1 stabilize ClC-2 at the plasma membrane (28), we then measured ClC-2 protein levels. Similarly, ClC-2 protein levels were increased in the KO animals in a significative manner (Fig. 5A). In contrast, GPRC5B protein levels remained unchanged (Fig. 5A).

An increased signal was observed in tissue samples from KO animals when immunofluorescence experiments detecting MLC1 and GlialCAM at the Bergmann glia were performed. However, MLC proteins showed a more dotted pattern compared with WT signal (Fig. 5B). Similar results were observed for ClC-2 (Supplementary Material, Fig. S3A). Quantification of the fluorescent signal revealed increased amounts of MLC1 in *Gpr37l1* KO mice (Fig. 5B). Similarly, the fluorescent signal of MLC proteins was increased in primary astrocyte cultures from the KO mice (Supplementary Material, Fig. S3B). In contrast, the signal of GPRC5B in astrocyte cultures from KO animals remained unchanged (Supplementary Material, Fig. S3C).

To determine whether MLC1 subcellular localization was altered in *Gpr37l1* KO mice as the immunofluorescence staining suggested, we detected MLC1 by electron microscopy (EM) immunogold experiments (Fig. 5C). These experiments showed that the localization of MLC1 in Bergmann glia (Fig. 5Ca) or in perivascular astrocytic processes was not affected (Fig. 5Cb).

Similarly, we assessed whether the expression of GPR37L1 and GPRC5B depends on MLC1. Western blot experiments revealed that the total amount of GPR37L1 and GPRC5B was the same in the brain and the cerebellum of *Mlc1* KO mice (Supplementary Material, Fig. S4A and B). Likewise, there was no change in the subcellular localization of GPRC5B in the astrocytic endfeet around blood vessels in *Mlc1* KO mice (Supplementary Material, Fig. S4C).

We conclude that the lack of GPR37L1 in mice upregulates MLC protein levels without altering their localization. Moreover, no change is observed for GPRC5B protein.

Knockdown of GPRC5B in primary astrocytes downregulates MLC proteins

We next studied whether the lack of GPRC5B might influence MLC proteins. GPRC5B has been described to be expressed in neurons, oligodendrocytes and astrocytes (16). *Gprc5b* KO mice display gliosis and axonal swellings in the cerebellum caused by increased ROS (29,30). In order to avoid any secondary effect of the loss of GPRC5B, experiments addressing the cellular effects

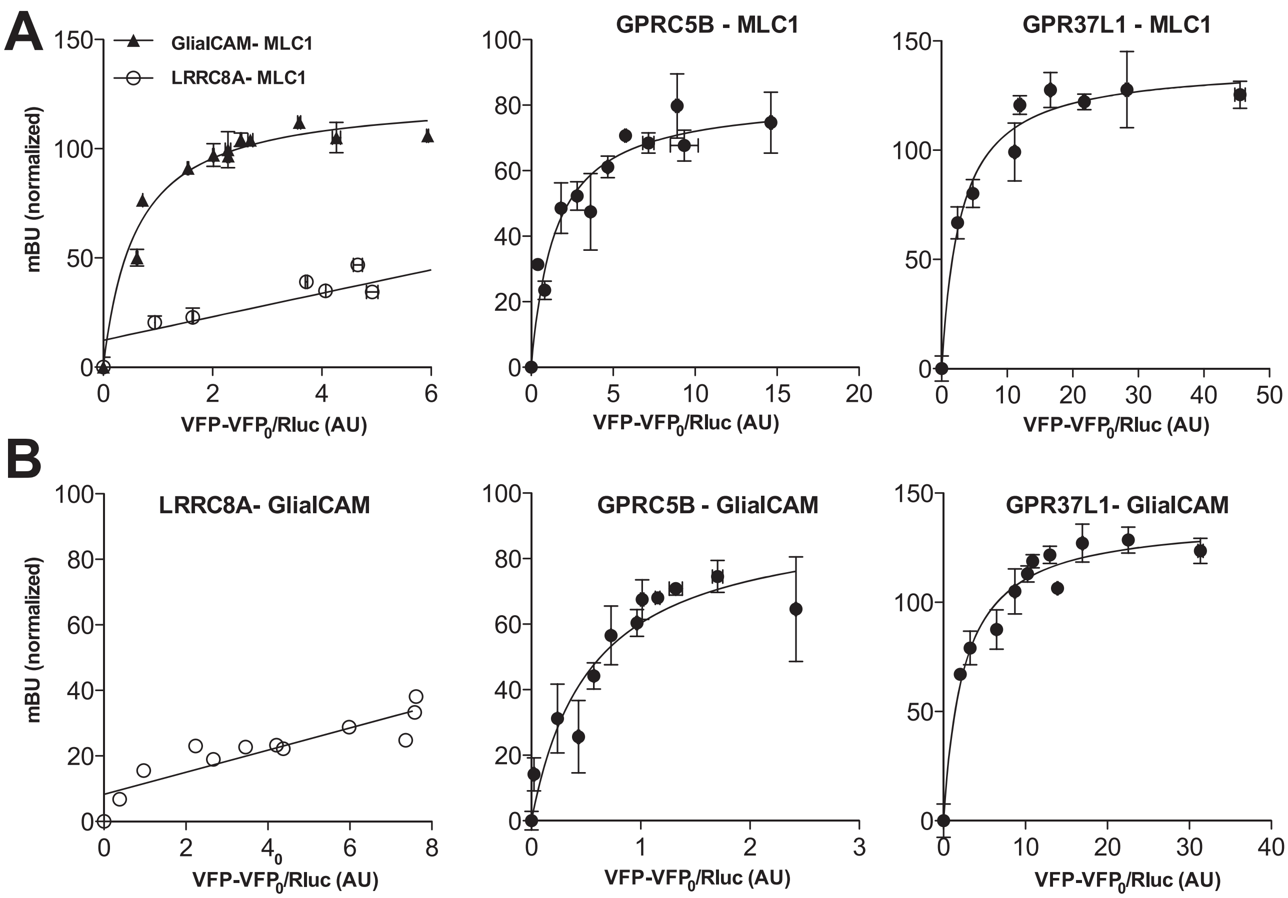

Figure 4. Direct interaction of the human GPCRs with human GlialCAM or human MLC1 by bioluminescence resonance energy transfer (BRET) assays. Representative BRET saturation curve between GPCRs and MLC1 (**A**) or GlialCAM (**B**) from 3 to 5 independent experiments. HEK293T cells were co-expressing a constant amount of GPRC5b-Rluc or GPR37L1-Rluc in presence of increasing concentrations of MLC1-VFP or GlialCAM-VFP. The interaction between GlialCAM-Rluc and MLC1-VFP were analyzed as positive control, and with human LRRC8A as negative control. Plotted on the x axis is the fluorescence value obtained from the VFP, normalized with the luminescence value of the Rluc constructs 10 min after coelenterazine h incubation and the y axis the corresponding BRET ratio (x1000). mBU: mBRET units. Results are expressed as mean ± standard error of mean.

of GPRC5B ablation on MLC proteins were therefore performed on primary cultured astrocytes. For this purpose, we developed adenoviral vectors expressing a shRNA against mouse *Gprc5b* (sh Gprc5b) that were able to nearly deplete GPRC5B levels (Supplementary Material, Figs S2B and C, and 6A). An adenoviral vector expressing a scrambled shRNA was used as control.

In GPRC5B-depleted astrocytes, MLC1 and ClC-2 total protein levels were significantly reduced. In contrast, GlialCAM and LRRC8A protein levels were not altered (Fig. 6A). Because our results have shown that GPRC5B interacts directly with MLC1 and GlialCAM, we reasoned that GPRC5B ablation could influence GlialCAM plasma membrane levels in the absence of MLC1. GPRC5B depletion reduced GlialCAM levels at the plasma membrane in *Mlc1* KO astrocytes (Fig. 6B). Immunofluorescence experiments indicated that GlialCAM was internalized in *Mlc1* KO astrocytes depleted of GPRC5B (Fig. 6C), suggesting that GPRC5B may stabilize GlialCAM at the plasma membrane. In these GPRC5B-depleted astrocytes, complementation with an adenovector expressing human MLC1 rescued GlialCAM localization at the plasma membrane (Fig. 6C), in agreement with previous studies that indicated that MLC1 also stabilizes GlialCAM (31). Hence, GPRC5B might stabilize both MLC1 and GlialCAM at the plasma membrane and thus, it may influence the activity of different chloride channels that have been linked to the presence of GlialCAM and MLC1 in depolarizing (ClC-2) or hypotonic (VRAC) conditions.

In agreement with this hypothesis, the ablation of GPRC5B almost completely abolished the localization of ClC-2 at cell–cell junctions in depolarizing conditions, with a drastic reduction from 47 ± 2 to 7 ± 3 (n = 3 experiments, 108 cells counted, $^{***}P < 0.001$) in GPRC5B depleted samples (Fig. 7A). Furthermore, whole cell patch-clamp experiments in rat astrocytes demonstrated that GPRC5B knockdown decreased ClC-2 current activation and prevented its change in rectification observed in depolarizing conditions (Fig. 7B and C), as observed in the measurements of the normalized current (Fig. 7C and D) and the rectification index (Fig. 7E), respectively. Previous studies using VRAC and ClC-2 inhibitors together with shRNA directed against ClC-2 demonstrated that the chloride currents observed in depolarizing conditions are mediated by ClC-2 associated with GlialCAM and MLC1 (23).

Next, we measured VRAC activation by hypotonicity in GPRC5B-depleted astrocytes (Fig. 7F–H). Reduction of GPRC5B expression led to a dramatic reduction of VRAC current measured in hypotonic conditions (Fig. 7F–H).

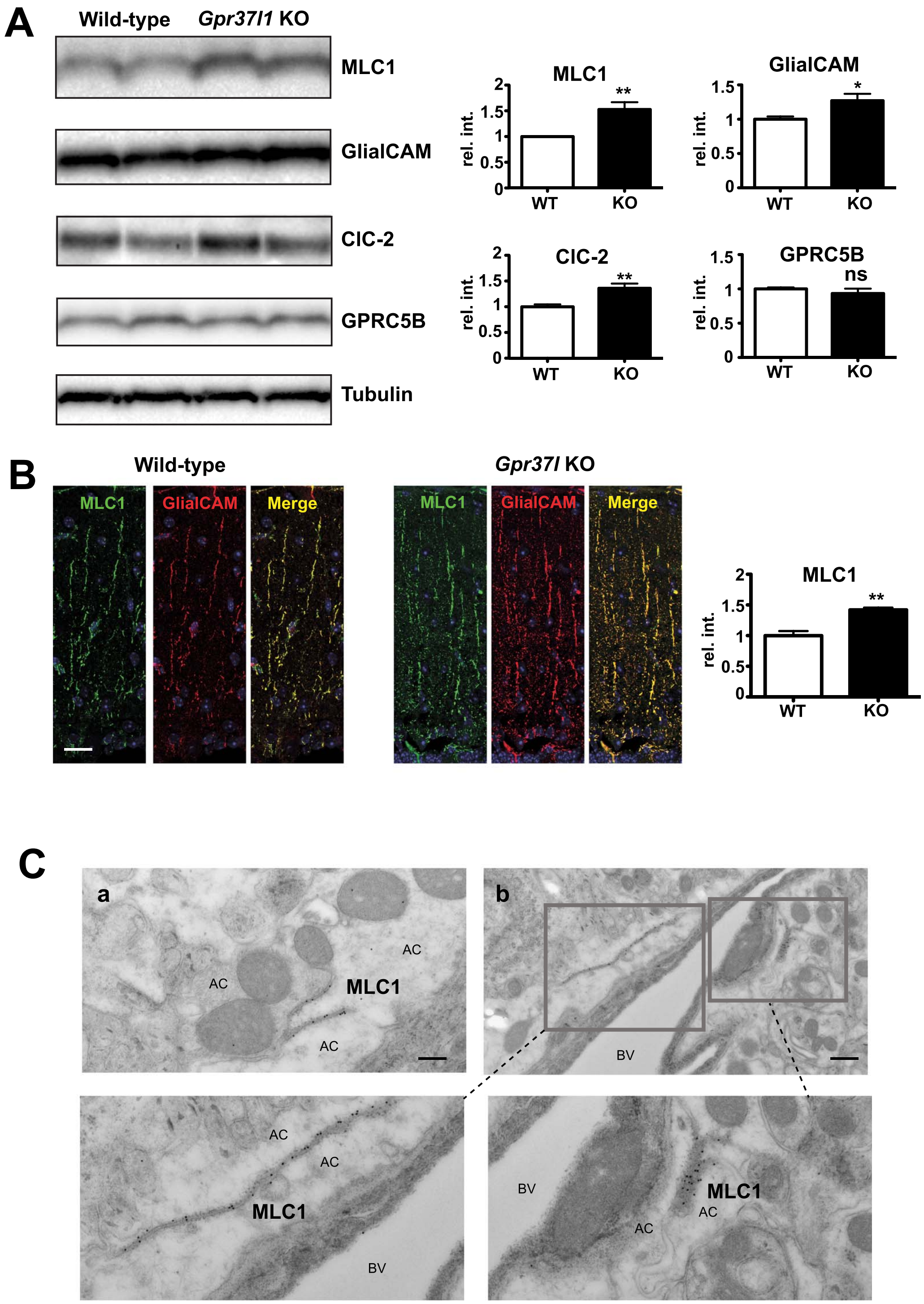

Figure 5. Expression and localization of MLC proteins in *Gpr37l1* KO mice. (**A**) Representative Western blot analysis and densitometric quantification in whole cerebellar extracts from wild-type (WT) and *Gpr37l1* KO adult mice. Data are expressed in arbitrary units (rel.int.: relative intensity) as a ratio to the mean values obtained from WT mice (unpaired *t*-test; $^{*}P < 0.035$; $^{**}P < 0.007$, $n = 6, 7$). (**B**) Representative confocal images of MLC1 (green), GlialCAM (red) co-immunofluorescence labeling and DAPI staining (blue) in cerebellar sections of WT and adult mice (left). Scale bar, 20 µm. The quantification of MLC1 immunostaining intensity (right). Data are expressed in arbitrary units as a ratio to the mean values obtained from WT mice (unpaired *t*-test; $^{**}P \leq 0.0070$; $n = 3$). (**C**) At EM level, MLC1 post-embedding staining in *Gpr37l1* KO showed immunoreactivity in the astrocyte–astrocyte junctions of protoplasmic (a) and perivascular (b) astroglial processes. AC, astrocyte; BV, blood vessel. Higher magnifications of boxed areas (dashed lines) in (b) are presented. Scale bar, a: 0.25 µm; b: 0.5 µm.

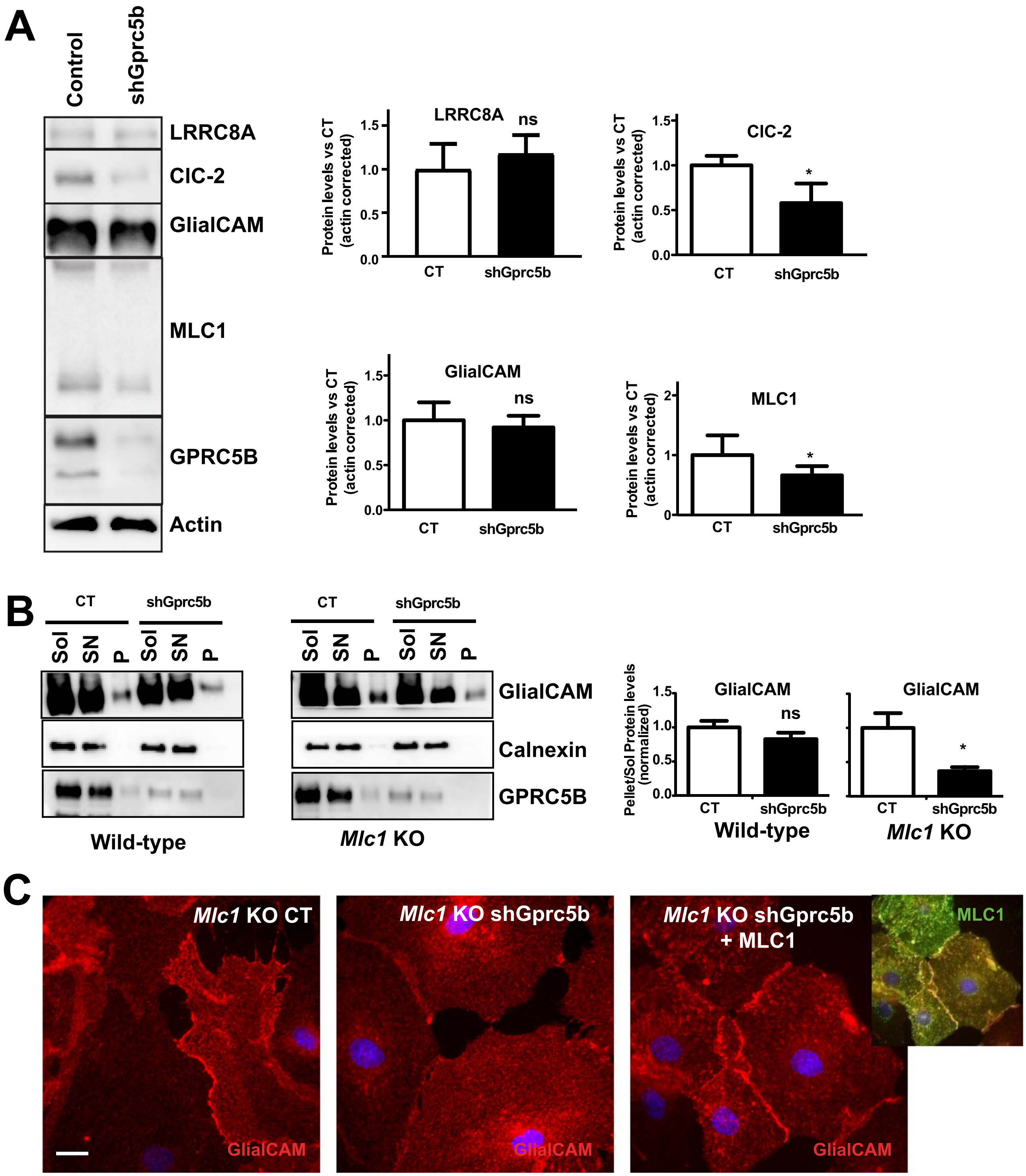

Figure 6. Characterization of GPRC5B depleted primary astrocytes. (**A**) Total protein levels of MLC1, GlialCAM, ClC-2 and LRRC8A were assessed by Western blot (left) in extracts obtained from arrested astrocytes control or infected with shRNA against *Gprc5b*. β-actin was used as a loading control, and GPRC5B was detected to validate the effect of the shRNA. The result shown is representative of four independent experiments. The quantification of these different experiments (right) revealed a decrease in protein levels in the case of ClC-2 and MLC1. *$P < 0.05$ in the Student *t*-test of shRNA versus control. (**B**) Surface levels of GlialCAM in GPRC5B depleted primary astrocytes from wild-type or *Mlc1* KO mice were assessed by biotinylation and subsequent Western blot of the solubilized extract (sol), the supernantant of the purification (SN) and the purification (P). Quantification of the biotynilated fraction (P) revealed a decrease in GlialCAM membrane protein levels only in *Mlc1* KO astrocytes. *$P < 0.05$ in the Student *t*-test of shRNA versus control. Calnexin was detected as a non-plasma membrane (ER) resident protein. (**C**) The misslocalization of GlialCAM in GPRC5B depleted astrocytes from *Mlc1* KO mice is corrected by complementation with human MLC1 overexpressing adenovirus (right). Scale bar: 20 μm. ns, not significant.

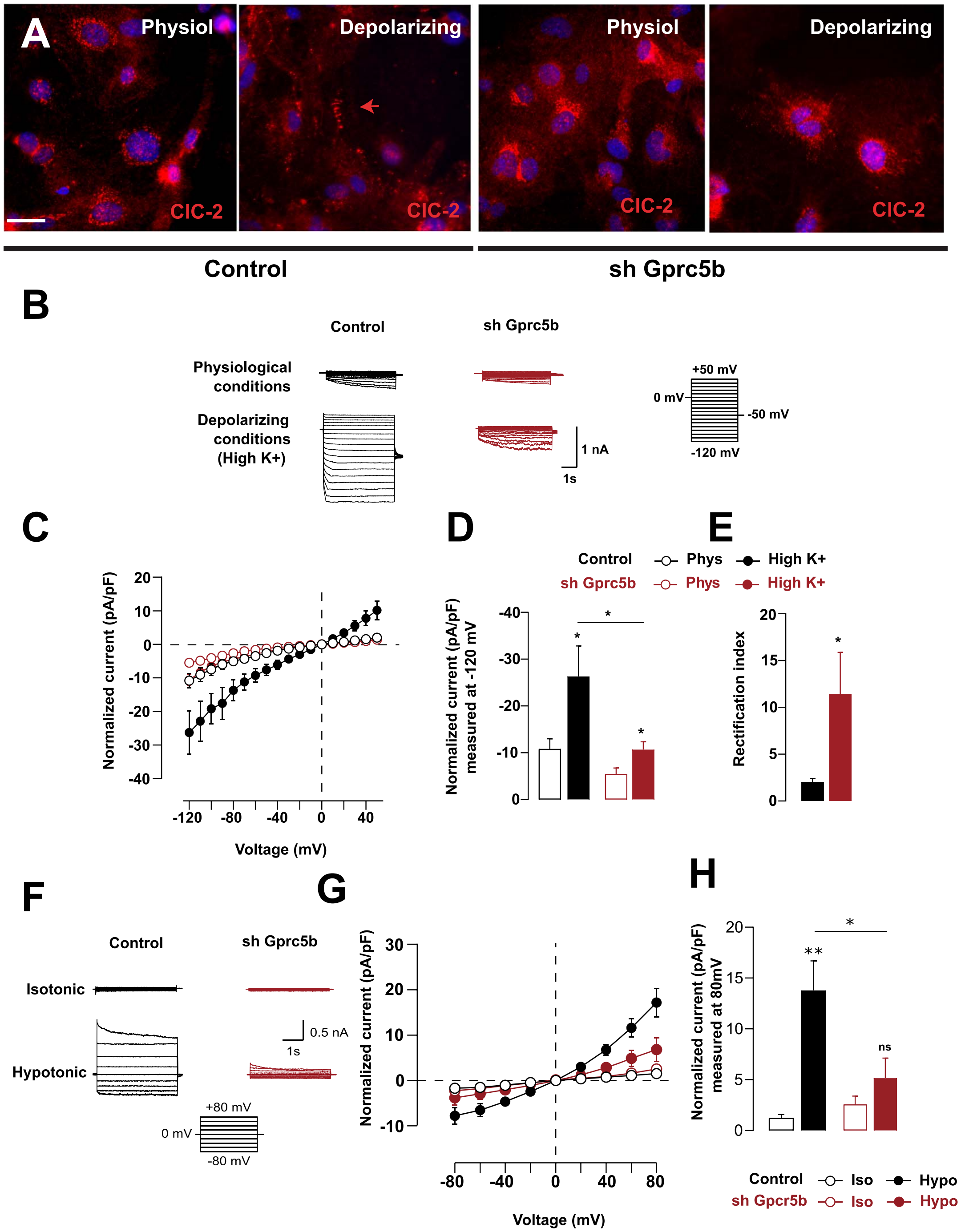

Figure 7. Lack of GPRC5B affects ClC-2 and VRAC activation in depolarizing and hypotonic conditions. (**A**) Immunostainings of ClC-2 in Control or GPRC5B depleted astrocytes treated with physiological or depolarizing solutions. GPRC5B depleted astrocytes showed a markedly reduced ClC-2 trafficking to cell–cell junctions in depolarizing conditions (arrows). $^{***}P < 0.001$ in one-way analysis of variance plus Dunnet multiple comparisons' test versus the depolarizing control. (**B–E**) Reduced activation in depolarizing conditions of the ClC-2 chloride channel in GPRC5B depleted astrocytes. (B) Representative whole-cell recordings from control and GPRC5B-depleted rat astrocytes showing ClC-2 currents evoked by voltage pulses (from −120 to +50 mV) in both physiological and depolarizing conditions. The protocol applied is depicted on the right. (C–E) Current-voltage relationships show the previously described increase in ClC-2 currents when astrocytes are treated with a depolarizing solution and a change in the rectification index. In GPRC5B-depleted astrocytes, however, this increase in the current amplitude is much smaller and no changes in the rectification index can be observed. Quantification of the current measured at −120 mV in both control and GPRC5B-depleted astrocytes can be seen in (D) and changes in the rectification index are depicted in (E). Whole-cell currents shown in (C) and (D) are normalized by cell capacitance. $^{*}P < 0.05$, $^{**}P < 0.01$. The number of experiments is Control phys = 20, Control depolarizing = 14, sh Gprc5b phys = 9, shGprc5b = 11. (**F–H**). (F) Representative whole-cell recordings from control and GPRC5B-depleted rat astrocytes showing VRAC currents evoked by voltage pulses (from −80 to +80 mV) before and after 5 min of hypotonic stimulation. The protocol applied is depicted in the middle. (G and H) Current-voltage relationships showed that current activation upon hypotonicity was not statistically significant in GPRC5B-depleted astrocytes and VRAC currents from these cells were much smaller when compared with those of control astrocytes. Quantification of the current measured at +80 mV can be seen in (H). Whole-cell currents shown in (G) and (H) are normalized by cell capacitance. ns, not significant, $^{*}P < 0.05$, $^{**}P < 0.01$. The number of experiments is Control = 12, sh Gprc5b = 8.

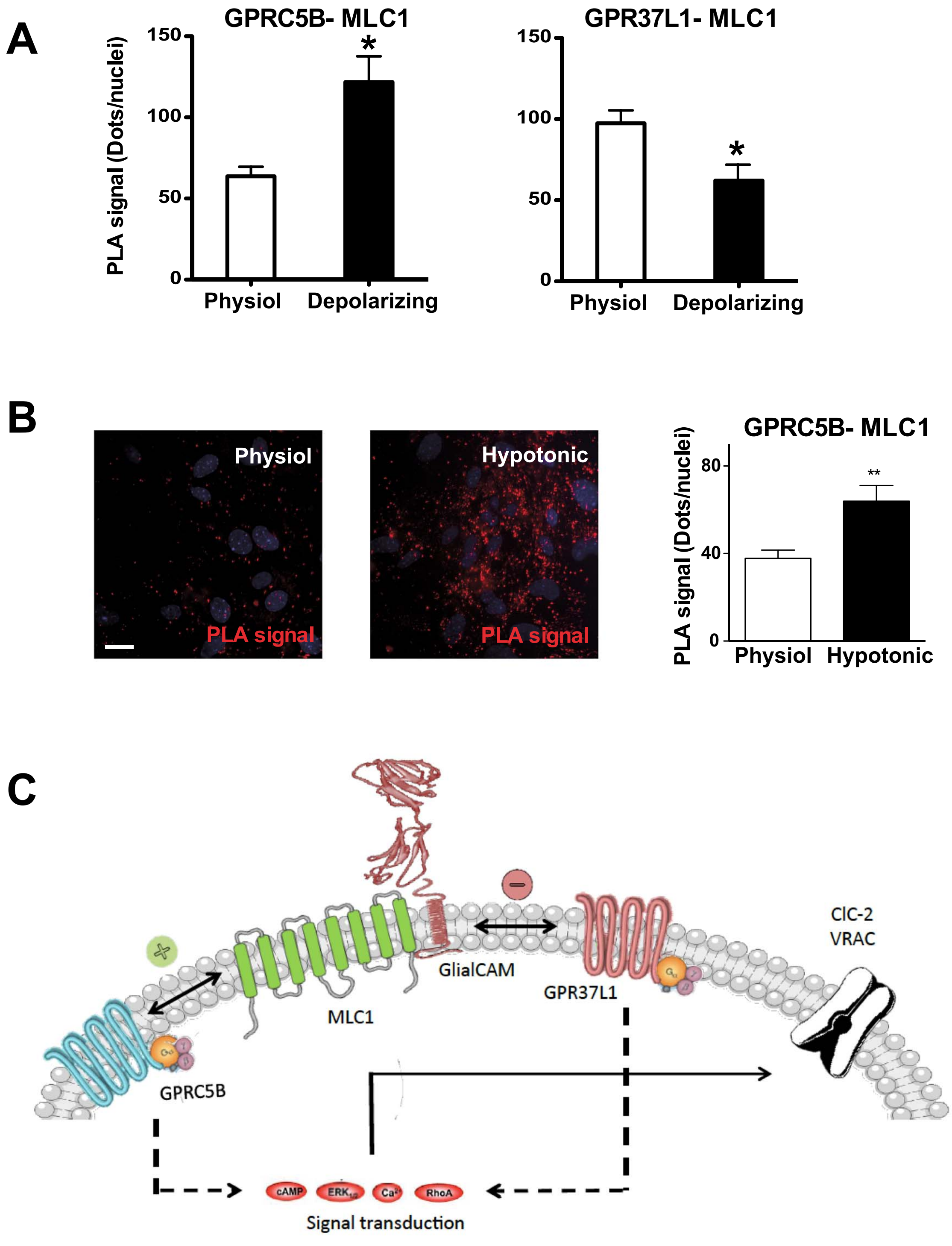

Figure 8. Depolarization and hypotonicity dynamically modulate the interactions between MLC1 and GPCRs. (**A**) The interaction of MLC1 and the GPCRs in depolarizing conditions. Astrocytes were treated with physiological or depolarizing solutions for 4 h, and then PLA between MLC1 and GPRC5B (left) or GPR37L1 (right) was assessed. The number of PLA positive dots was normalized by the negative control and quantified using Image J. Data are mean ± standard error of the mean of three-four independent experiments. $*P < 0.05$ in the Student *t*-test of depolarizing versus physiological conditions. (**B**) The interaction between GPRC5B and MLC1 protein measured by PLA increased by hypotonicity. Wild-type (WT) or *Mlc1* KO mouse cultured astrocytes were treated with physiological or hypotonic solution for 15 min, and then PLA assay between GPRC5B and MLC1 was performed. Assays were performed with mouse monoclonal anti-MLC1 and rabbit polyclonal anti-GPRC5B. *Mlc1* KO mouse astrocytes were used as negative control. Data analyses were from three independent experiments and were corrected subtracting the signal of the negative control. $^{**}P < 0.001$ in two-tailed Student *t*-test. (**C**) Model of the interplay between MLC proteins and two of the GPCRs identified in the GlialCAM interactome. In this model, GlialCAM and MLC1 are negatively and positively regulated by GPR37L1 and GPRC5B, respectively. The interaction between the GPCRs and MLC proteins might activate signal transduction cascades previously linked to Mlc1 or these GPCRs (such as cAMP, ERK1/2, Calcium or RhoA), which will regulate different transporters and channels, as illustrated by the effects seen in this work over the ClC-2 and the VRAC chloride channels.

Depolarization and hipotonicity modulates GPCRs-MLC1 protein interaction

The above results suggested that the lack of GPR37L1 increases MLC proteins levels, whereas the opposite was observed for the lack of GPRC5B. This suggests that these GPCRs may interact with MLC proteins in a dynamic manner. Previous studies indicated that the interaction between GlialCAM/MLC1 and ClC-2 in primary cultured astrocytes was dynamically regulated, and it was observed on depolarizing conditions (23).

Then, we compared the interaction between GPRC5B or GPR37L1 with MLC1 in physiological versus depolarizing conditions in primary astrocyte cultures. PLA indicated that the interaction between MLC1 and GPRC5B was increased in depolarizing conditions whereas the interaction between GPR37L1 and MLC1 was decreased (Fig. 8A). Therefore, these experiments suggested that in depolarizing conditions GPRC5B might be needed for signal transduction responses in a GlialCAM/MLC1-dependent manner.

Subsequently, we assessed whether the interaction between MLC1 and GPRC5B also varies in hypotonic conditions performing PLA. We observed that the interaction between both proteins increased under hypotonic conditions (Fig. 8B).

Discussion

GlialCAM and MLC1 are two membrane proteins linked to a human genetic disease (MLC) and whose biological functions are poorly understood. Previous studies suggested that they might have a role in astrocyte ion/water homeostasis by influencing different ion channels and transporters. In this respect, a direct interaction after astrocyte despolarization has been observed with the chloride channel ClC-2 and it has also been shown to influence VRAC chloride channels and regulatory volume decrease after astrocyte osmotic swelling in an indirect manner. In addition, it has been shown that the overexpression of MLC1 downregulates intracellular signaling pathways controlling astrocyte activation and proliferation. In order to get more insights into the biological role of GlialCAM and MLC1, we have identified GlialCAM-interacting proteins and their association with MLC1 by means of immunoprecipitation and MYTH experiments. Our results revealed that GlialCAM forms a network of $\sim$20 proteins.

Within this proteome there are different proteins, some of them previously identified (such as ClC-2, Cx43 or Na^+/K^+-ATPase), which are related to ion or substrate transport and are involved in the homeostasis of the extracellular media during neuronal activity. Neuronal activity in the central nervous system leads to an increase of potassium in the extracellular space (32). This increase is rapidly buffered by neighboring astrocytes through different molecular mechanisms, including the activity of pumps, transporters and ion channels. One of the most important processes contributing to potassium clearance is its uptake by astrocytes mediated by the Na^+/K^+-ATPase (33). Moreover, the ATPase is activated by intracellular increases in sodium, as occurs in astrocytes during neuronal activity because sodium-coupled glutamate transporters, mainly EAAT2 (or GLT-1) and EAAT1 (or GLAST), remove neurotransmitters from the extracellular media. Potassium may also enter into astrocytes through potassium channels, mainly Kir4.1 (34). Potassium would diffuse to neighboring astrocytes through gap junctions [composed by connexins 30 and 43 (Cx30 and Cx43)] (35,36) in a process that has been defined as spatial buffering (37,38). In addition, potassium can be accumulated inside astrocytes, which is balanced by a parallel transport of chloride to maintain electroneutrality (39). In this case, it has been suggested that chloride might enter astrocytes through ClC-2 chloride channels in association with GlialCAM/MLC1 proteins (10). Within other proteins belonging to the same group of transporter/ion channels, it is interesting to mention the sodium-driven bicarbonate transporter (NBCe1). Astrocytes contribute to the reacidification or basification of the extracellular media during neuronal activity, partly through the activation of NBCe1 (40).

The results presented here suggest that GlialCAM/MLC1 form a protein scaffold for different transporters and ion channels involved in neuronal homeostasis. Previous work has shown that GlialCAM is able to target ClC-2 to glial junctions and modify its gating properties (9). It remains unknown if GlialCAM is also able to modify the functional properties and the localization of the identified proteins. Hence, MLC disease could be caused by impaired activity of some of the proteins found in the GlialCAM interactome.

On the other hand, GlialCAM and MLC1 have been shown to influence intracellular signaling pathways controlling astrocyte activation and proliferation. Several proteins have been identified related to cell signaling within this proteome, such as three different GPCRs (GPR37, GPR37L1 and GPRC5B), a tetraspanin (CD9) (41) and the four transmembrane domain proteins Glycoprotein M6A and M6B (42,43). Considering the role played by GPCRs, we hypothesize that some of the signaling pathways involving MLC proteins might be caused by the activity of these GPCRs.

Within the identified GPCRs, GPR37 and GPR37L1 are part of the rhodopsin (Class A) family, specifically within the endothelin B receptor-like peptide family (44–47). Both GPCRs are highly expressed in the central nervous system. GPR37 is mainly expressed in oligodendrocytes, whereas GPR37L1 is mainly expressed in astrocytes with higher levels in the Bergmann glia of the cerebellum. Studies with KO mice have shown that GPR37 regulates negatively oligodendrocyte differentiation and myelination (21), and that GPR37L1 participates in regulating the development of neuronal and glial cells in the cerebellum (22). Several groups have proposed that prosaposin and derived prosaptides could bind to these GPCRs and activate them, but *in vitro* studies with induced expression of both proteins have so far failed to conclusively prove that these are the cognate ligands (17,19,48–50). It has been indicated that GPR37 and GPR37L1 are coupled to $G\alpha_{i/o}$, which will inhibit adenylate cyclase. Thus, the lack of these GPCRs results in increased cAMP levels and Epac-dependent activation of MAPK cascade, which leads to an increase in phospho-ERK1/2 (21,51). In this sense, *Mlc1* KO cells also show an increase in ERK phosphorylation and its expression is also linked to astrocyte differentiation.

GPRC5B belongs to the family C group IV (metabotropic glutamate receptor-like receptor) of GPCRs (16). GPRC5B is expressed ubiquitously, particularly in the brain, mostly in the cerebellum, adipose tissue and placenta (29). It is subcellularly localized at the plasma membrane, Golgi and exosomes (52). GPRC5B has been implicated in neuronal cell-fate determination, cerebellar motor learning, obesity and inflammation (53–56). There is not a known ligand neither a G protein coupled for GPRC5B, but it seems to recruit the Src-family kinase Fyn through the SH2 domain during its activation, and the activity of Fyn regulates inflammatory responses via NF-kB signaling (53,57). Considering MLC, it has been found that in astrocytoma, the overexpression of MLC1 inhibit the activation of IL-1β-induced inflammatory signals (pERK, pNF-kB) that, conversely, were abnormally upregulated in *Mlc1* KO astrocytes (58).

Thus, considering previous data and the present work, we suggest that these GPCRs could participate in the signaling role previously assigned to GlialCAM and MLC1 (Fig. 8C). First, we have observed that the lack of GPR37L1 upregulates GlialCAM and MLC1 whereas the lack of GPRC5B downregulates it, influencing ClC-2 and VRAC activity. As GPRC5B interacts more with MLC1 in depolarizing and hypotonic conditions, the activity of GPRC5B might be important in metabolic processes related to changes in the ionic composition. In contrast, we hypothesize that signaling through GPR37L1 might be related to differentiation processes. Although future research is needed to understand how GlialCAM and MLC1 modulate GPCR-associated signaling processes, taking into account that they interact *in vitro*, it is possible that they might regulate the activation of the GPCRs through lateral interactions.

Although the exact role played by GlialCAM and MLC1 is still unknown, this work has revealed that the role played by MLC1 is very similar to the work performed by tetraspanins. Tetraspanins are transmembrane proteins that span the plasma membrane four times and that associate with other tetraspanins by homo- and heterooligomerization (59). It has been described in many cases that they form a tight complex with a single-pass transmembrane protein belonging to the immunoglobulin (Ig) superfamily (60). For instance, the tetraspanin CD81 is associated with CD19 (61) or the tetraspanin CD9 with EWI-2 (62). Moreover, these molecules can simultaneously associate laterally at the plasma membrane with numerous integral membrane receptors, modulating their functions and organizing discrete, dynamic plasma membrane compartments (63). Within these partners, there are GPCRs (64) or other cytoplasmatic signaling mediators (65). They might also regulate the trafficking and biosynthetic processing of these partners (66). Considering MLC1, although the sequence homology to tetraspanins is very low (~20%), it passes the membrane eight times, but biochemical studies indicate that each four transmembrane domains can be considered as a duplicate (6). As tetraspanins, MLC1 also oligomerizes with himself and forms a tight complex with GlialCAM, a single-pass transmembrane domain of the Ig family (4). Here, we have also identified the tetraspanin CD9 as a protein forming part of the GlialCAM interactome and a direct interactor of MLC1. As tetraspanins, MLC1 influence the trafficking of diferent partners, as it has been shown for ClC-2 (9) or Cx43 (12). Finally, here we have shown that GlialCAM and MLC1 might be interacting with different GPCRs in a dynamic manner. Therefore, we propose that MLC1 biological role is that of being a tetraspanin-like molecule. Final proof of this hypothesis might need the determination of a 3D structure of the GlialCAM/MLC1 complex.

Understanding the interrelationship between GlialCAM/MLC1 and the GPCRs found here could be crucial not only to the development of therapies for MLC patients but also to unravel the mechanisms conducted by astrocytes to control neuronal homeostasis. In this sense, analyses of the posttranslational modifications of the interactome proteins identified here in MLC mice models as in the *Glialcam* KO, could provide novel insights into regulatory mechanisms. It would be interesting to analyze if the minor percentage of MLC patients without mutations in *GLIALCAM* or *MLC1* harbor mutations in any of the genes coding for the GPCRs identified here.

Materials and Methods

Molecular biology

Plasmids presented herein were constructed using standard molecular biology techniques employing recombinant PCR and the Multisite Gateway System (Invitrogen). The integrity of all cloned constructs was confirmed by DNA sequencing.

Animal procedures

The generation of *Glialcam*$^{-/-}$ and *Mlc1*$^{-/-}$ mice has been previously described (10). *Gpr37l1*$^{-/-}$ mice has also been previously characterized (22). For histological analyses of brains, mice were perfused with 4% PFA/PBS and organs were postfixed overnight. Mouse astrocyte cultures were performed from P0 to P2 mouse pups of the corresponding genotype as previously described (31).

Membrane preparation

Fresh-frozen brains from mouse WT and *Glialcam* KO were homogenized with a glass potter in sucrose buffer (320 mM sucrose, 10 mM Tris, 2 mM $MgCl_2$, 1 mM EGTA, protease inhibitors (5×), pH 7.5; ca. 10 ml/g tissue) and centrifuged for 5 min at 1080 × g. The supernatant (SN) was collected and the procedure was repeated with the pellet using a third of the sucrose buffer volume. Both supernatants were combined and ultracentrifuged (10 min at 200,000 ×g) to collect the crude membrane pellet. The crude membrane pellet was resuspended in hypotonic buffer (50 mM Tris/HCl pH 7.5) and allowed to lyse for 30 min on ice (with gentle stirring). The membrane lysate was then separated on a sucrose step gradient (10 ml 1.3 M sucrose and 10 ml 0.5 M sucrose, each in 10 mM Tris–HCl/1 mM Mg^{2+}/pH 7.5) for 1 h at 200,000 × g. The interface band was collected, diluted 3-fold with 20 mM Tris–HCl/1 mM Mg^{2+}/pH 7.5 and pelleted by ultracentrifugation. The pellets were resuspended in a small volume of 10 mM Tris–HCl/1 mM Mg^{2+}/pH 7.5 and the protein concentration was determined by the Bradford method.

Solubilization and AP

AP was carried out with CL47 supplemented with 1 mM Mg^{2+}. In addition to mouse WT and *Glialcam* KO membranes, a rat brain membrane preparation was used. For each purification experiment, 20 µg of immobilized antibody were incubated with 2 mg membrane solubilized with 1.6 ml CL47 (+1 mM Mg^{2+} and 4× protease inhibitors added). Solubilization was carried out at a protein-detergent ratio of 1:8, incubated for 20 min on ice and cleared by ultracentrifugation at 56,000 rpm/12 min (rotor Sorvall S80-AT3; corresponding to a 200 S cutoff for solubilized particles). After 2 h of incubation with the solubilisate antibodies were washed with CL47 dilution buffer 1 mM Mg^{2+} (2 × 1 ml for 5 min) and eluted with 2 × 7 µl non-reducing Lämmli buffer (100 mM DTT added later).

MS sample preparation and LC-MS/MS analysis

The eluates from APs were shortly run on 10% SDS-PAGE gels and silver-stained. Lanes were excised and split into two parts (> and <50 kDa), each subjected to standard in-gel tryptic digestion. Eluted peptides were vacuum-dried and redissolved in 13 µl 0.5% trifluoroacetic acid prior to MS analysis.

For comprehensive LC-MS/MS analysis, peptides were loaded on a C18 PepMap100 precolumn (5 µm; Dionex) and resolved on an analytical 75 µm × 10 cm C18 column (PicoTip™ Emitter, 75 µm, tip: 8 ± 1 µm, New Objective; self-packed with ReproSilpur 120 ODS-3, 3 µm, Dr Maisch) using an aqueous-organic gradient [UltiMate 3000 HPLC coupled to an Orbitrap XL mass spectrometer (Thermo Scientific)]. Full spectra (with precursor signals used for quantification) were acquired with a target value of 500 000 and a nominal resolution of 60 000 (scan range 370–1700 m/z).

Up to five data-dependent collision-induced dissociation (CID) fragment spectra per scan cycle were acquired in the ion trap with a target value of 10 000 with dynamic exclusion, preview mode for full precursor scans, charge state screening, monoisotopic precursor selection and rejection charge state 1 enabled. Activation type was CID with default settings.

LC-MS/MS data were extracted and searched against the UniProt Knowledgebase (mouse, rat, human and release 2013-09) using the Mascot search engine (version 2.3.01; Matrix Science) together with anti-GlialCAM AP datasets from a previous round of experiments. For preliminary searches peptide mass tolerance was set to 15 ppm. After linear shift mass recalibration the window was narrowed to $\pm$ 5 ppm for final searches. Fragment mass tolerance was set to 0.8 Da. One missed trypsin cleavage and common variable modifications were accepted for peptide identification. Proteins identified by only one specific MS/MS spectrum or representing exogenous contaminations such as keratins or Igs were eliminated.

Analysis of GlialCAM and MLC1 interaction partners

The set of GlialCAM-APs (total of 14) was quantitatively evaluated together with an AP data set from an older experiment (previous study, 4 samples). A label-free evaluation pipeline similar to (67) was used. Briefly, m/z features among LC-MS scans were detected and their intensitied integrated (as intensity $\times$ retention time $\times$ m/z width = PV) using MaxQuant (Cox and Mann 2008, version 1.3). m/z-corrected features were then aligned between different LC-MS/MS runs and assigned to the peptides identified by Mascot using a home-written software tool with mass tolerance set to 1.5 ppm and a time shift window of 1 min. The resulting assignment showed an even distribution with very high m/z precision and no obvious systematic error (symmetric, no offsets from 0 in either dimension).

Based on the accurately assigned PVs, protein abundance ratios (rPV) in purifications from WT versus control (IgG or *Glialcam* KO) were determined using the TopCorr method (68). Protein-specific peptide PVs were ranked across the evaluated datasets by their consistency using pair-wise linear correlation analysis (Pearson correlation). A maximum of six to a minimum of two peptide PVs were then selected from the best correlating PVs to calculate the abundance ratio as median of the respective peptide PV ratios (referred to as rPV). To ensure validity, sequenced peptides with missed PV assignment were omitted and a minimum of two peptide ratios with total assigned PVs of 80 000 units were required; if no PV could be assigned to a peptide in the AP controls, the detection limit of the spectrometer (3000 PV units with the settings used here) was inserted as a minimum estimate. Distributions of protein rPV values were plotted for each sample pair to derive specificity thresholds. Proteins were considered specifically co-purified when rPV (vs IgG) $>$ threshold (IgG) in both, rat and mouse, and no cross-reactivity was indicated by rPV(vs KO) $<$ threshold (vs KO). For each protein, the consistency of enrichment was evaluated with the different antibodies as well as its quantitative correlation with the purified target GlialCAM_Mouse [based on abundance$_{norm}$ values, (68)].

Finally, the LC-MS/MS data from previous Mlc1 AP experiments were reprocessed and evaluated according to the same improved procedures as described above. Because these datasets did not include target KO controls, specificity could not be evaluated with the same degree of stringency. Rather high thresholds (factor 20–60) for purification rPVs versus IgG were therefore applied.

MYTH screenings

A MYTH screening was performed with the biotech Dualsystems, using the bait vector pBT3-Ste containing human MLC1. A second screening was performed using the human brain DUALmembrane cDNA library in the NubG-x orientation as described (69).

Cell culture and transfection

Human embryonic kidney HEK-293T cells were grown at 37°C in an atmosphere of 5% CO_2 in Dulbecco's modified Eagle's medium (Sigma-Aldrich, St. Louis, MO, USA) supplemented with 1 mM sodium pyruvate, 2 mM L-glutamine, 100 U/mL streptomycin, 100 mg/mL penicillin and 5% (v/v) fetal bovine serum. The cells were seeded into six-well plates containing poly-D-lysine-coated glass coverslips at ~300 000 cells/well. Cells were transiently transfected with the corresponding cDNA constructs using Transfectin™ (Bio-Rad, Hercules CA, USA) and following the manufacturer's instructions.

Immunological procedures

For immunofluorescence staining, primary cells and tissue sections were fixed and processed as previously described (20,70). The polyclonal rabbit antibodies used were the following: anti-GlialCAM (1:100) (4), anti-MLC1 (1:100) (71), anti-ClC-2 (1:100) (9), anti-LRRC8A (1:100) (A304-175-A, Bethyl antibodies) (15) and the antibody developed in this work anti-GPRC5B against the peptide (C)TIPTAPPSHTGRHHW, using the services provided by Eurogentec. We also used a mouse monoclonal antibody that was developed against the mouse peptide sequence of the N terminus of MLC1 (TREGQFREELGYDRM) (23) and a mouse monoclonal specific for GPR37L1 (1:50 in mouse primary astrocytes, 1:100 in mouse tissue sections, Mab Technologies, Cat. N. scB12). GPR37L1 and MLC1 co-immunostaining was performed in mouse primary astrocytes from *Gpr37l1* WT and KO pups (51), after fixation with 100% methanol at -20°C for 20 min, permeabilizing with 0.1% Triton X-100 and incubating for 1 h at room temperature in blocking buffer containing 0.5% BSA, 0.3 M glycine (Merck, Cat# 104201) and 0.1% Tween-20.

For electron immunogold experiments, small samples of *Gpr37l1* cerebellum KO mice tissue were obtained and fixed in 4% paraformaldehyde and 0.1% glutaraldehyde in 0.12 m phosphate buffer, and processed. They were cryoprotected gradually in sucrose and cryofixed by immersion in liquid propane. Freeze substitution was performed at −90°C during 3 days in an Automatic Freeze Substitution System (AFS, Leica); methanol containing 0.5% uranylacetate was used as a substitution medium. Infiltration was carried out in Lowicryl HM20 at −50°C and then polymerized with UV light. Ultrathin sections were collected, and when needed, processed for post embedding immunostaining. For immunostaining, grids were incubated with rabbit anti-MLC1 (1:10) or antisera. The binding of the primary antibody was visualized by incubating with a secondary antibody conjugated to 18 nm gold particles (British BioCell, International).

In the western blot studies, astrocyte lysates and cerebellar extracts were prepared and processed as previously described

(20,72). The mouse GPR37L1 protein was detected with a goat polyclonal antibody (1:500, Santa Cruz, Cat. N. sc-164532). β-actin or α-tubulin proteins were used as a loading control.

To detect surface levels of GlialCAM, WT or *Mlc1* KO mouse astrocytes were cultured in 6 cm plates. They were washed 3 times with PBS-CM (PBS with 1 mM $CaCl_2$ and 1 mM $MgCl_2$). Subsequently, the astrocytes were incubated on ice for 30 min in PBS-CM containing 2 mg/ml EZ-LinkTM Sulfo-NHS-Biotin (Thermo Scientific). After three washes with PBS-CM, they were quenched for 10 min in PBS Ca/Mg containing 10 mM Lysine. After three additional washes with PBS-CM, the cells were lysed in RIPA buffer (50 mM Tris pH 8, 150 mM NaCl, 1% NP-40, 0.5% deoxycholate, 0.1% SDS, 2 mM EDTA) containing protease inhibitors, for 1 h. After centrifugation for 15 min at 14 000 rpm, the lysate was quantified using the BCA protein assay (Thermo Fisher). Then 2 mg of the solubilized extract in a total volume of 200 μl was incubated with 100 μl of streptavidin agarose (Thermo Fisher) O/N at 4°C. After a brief centrifugation, the SN was taken and the beads were washed three times with RIPA buffer. Biotinylated proteins were eluted with LSB 1× for 15 min at 60°C. Samples of lysate, SN and eluate were analyzed by western blot. To confirm that only membrane proteins were detected in the eluate, we performed a western blot with antibodies to test for the protein calnexin resident in the endoplasmic reticulum.

GVUs purification

GVUs were isolated from whole WT OF1 brains as previously described (24). A selective filtration was performed to enrich vessels of 20 to 100 am diameter (24). For immunostaining, GVUs were plated on a glass slide coated with Cell Tak (Corning, Corning, NY, USA) and fixed in PBS/PFA 4% for 15 min at room temperature. GVUs were immersed in the blocking solution (PBS/NGS 5%/Triton X-100 0.5%) for 1 h at room temperature and incubated with primary antibodies and Isolectin GS-B4 (IB4) diluted in the blocking solution 12 h at 4°C. After 3 PBS washes, slices or GVUs were incubated 2 h at room temperature with secondary antibodies, rinsed in PBS and finally embedded in Fluormount G. GVUs were analyzed using a 63X objective on a confocal microscope.

Quantification of immunofluorescence and western blot labeling

Quantitative analysis of immunofluorescence signals was performed with the Imaris 5.0.2 software (Bitplane). Experiments were carried out with tissue samples obtained from three mice per genotype. Sections of similar size in similar regions were chosen and analyzed. All measurements were performed with the observer blind to the identity of the slides.

Quantification of western blot immunoreactive bands was performed with the Chemidoc XRS+ imager and Image Lab software (Bio-Rad). Experiments were carried out with tissue extracts obtained from six to seven mice per genotype. The intensity of each band was normalized to the intensity of the corresponding α-tubulin band. The average values of each experimental group were expressed in arbitrary units, as a ratio to the mean values obtained from the WT groups.

Primary astrocyte culture, adenoviral transduction and RNA interference

Rat primary quiescent astrocyte cultures were prepared as described previously (20) and maintained in culture in the presence of the mitotic inhibitor AraC for biochemical studies. Dibutyryl-cAMP (dBcAMP) differentiated rat astrocytes obtained as described elsewhere (73), were used for electrophysiological measurements, because they express higher levels of ClC-2 currents and are easier to patch. Immunofluorescence experiments were performed on both types of cultures, with similar results. The physiological solution was: (in mM) NaCl 122, KCl 3.3, $MgSO_4$ 0.4, $CaCl_2$ 1.3, KH_2PO_4 1.2, HEPES 25, Glucose 10 and it had pH 7.4. The osmolarity was 290–300 mOsm and was adjusted with manitol using a vapor-pressure osmometer (Model 3320, Advanced Instruments). In the hypoosmolar solution the osmolarity was adjusted to 180 mOsm/kg. Adenovirus expressing HA-tagged MLC1, and the transduction of astrocytes has been described previously (4). RNAi entry-clone (Gateway, Invitrogen) vectors were prepared using the Block-it PolII miR RNAi EmGFP or the Block-it PolII miR RNAi expression vector kit following the manufacturer's instructions. Entry clones were recombined using LR clonase into the vector pAdVDEST-CMV/V5. Adenoviruses were produced and titrated using fluorescence microscopy detecting EmGFP, which is expressed together with the shRNA, or detecting the viral protein Ad-Hexon. The sequence of the oligo used to knock down mouse GPRC5B expression was: shRNA Gprc5b (shRNA111): 5′ TGGACTGGACCTTCTTCCTCA 3′.

Proximity-ligation assays

Mouse cultured astrocytes seeded on 24 well coverslips were treated with physiological, depolarizing (60 mM K^+) or hypotonic solutions and then were fixed with PFA 3%. Cells were blocked with PBS1x/0.1% Triton X-100/10% FBS for 2 h, and then incubated with the primary antibodies (Mouse monoclonal or Rabbit anti-MLC1 antibody 1:100; Rabbit polyclonal anti-GPRC5B antibody 1:100, Mouse monoclonal anti-GPR37L1 1:100) diluted in blocking solution for 1 h. After 3 washes of 10 min with blocking solution, cells were incubated with the anti-rabbit PLA (+) and the anti-mouse PLA (−) probes (Sigma) diluted 1/5 in blocking solution for 1 h in a 37°C humid chamber. Cells were washed twice with washing buffer A (Sigma) during 5 min. To ligate the PLA probes, cells were incubated in ligation buffer diluted 1/5 in water containing the ligase diluted 1/40 for 1 h in a 37°C humid chamber. After 2 washes with washing buffer A of 2 min, the amplification reaction was performed in ampli RED buffer diluted 1/5 in water containing the polymerase diluted 1/80 for 100 min in a 37°C humid chamber. Cells were washed twice with washing buffer B during 10 min, followed by an additional wash with washing buffer B diluted at 0.01% during 1 min. Finally, coverslips were mounted in DUOLINK DAPI medium and images were acquired using a CellR olympus microscope.

To quantify the PLA signal, images were analyzed using ImageJ (74). First, nuclei were identified and substracted. Then, images were transformed to 8 bit and converted to binary images using the threshold setup. The number of dots/particles corresponding to the PLA signal was quantified using the analyse particle command of the ImageJ submenu, considering that the size (2^) of the particles should be bigger than 5. For each image, we determined the number of dots divided by the number of nuclei.

BRET experiments

HEK293T cells were transfected with a constant amount of GPRC5B-Rluc (200 ng), GPR37L1-Rluc, GlialCAM-Rluc or LRRC8A-Rluc and increasing amounts of MLC1-VFP or GlialCAM-VFP.

Equal DNA ratios were maintained with co-transfection or the empty vector pCDNA3.1, which equilibrated the total amount of transfected DNA. Forty-eight hours post-transfection, cells were washed three times with PBS, detached and resuspended in Hanks balanced salt solution (Thermo Fisher Scientific). An aliquot was used to determine the protein concentrations via the BCA assay, to control the total amount of protein used in the assay. Accordingly, cells were diluted to a density corresponding to a final protein concentration of 600 ng/µl. Cell suspensions (corresponding to 20 µg protein) were distributed in duplicates into white and black 96-well microplates (#3600 and #3650; Corning, Stockholm, Sweden) for BRET[1] and fluorescence measurements, respectively. The substrate, h-coelenterazine (Molecular Probes, Eugene, OR, USA) was added at a 5 µM final concentration. After 1 min (BRET[1]) and 10 min (Rluc total), the signals were measured using the ClarioSTAR microplate reader (BMG Labtech, Ortenberg, Germany) through the sequential integration of signal detection at 475 nm (445–505 nm) and 530 nm (500–560 nm). The net BRET1 ratio was expressed as a ratio of the light intensity at 530 nm over 475 nm by substracting the background signal, which was detected when the Rluc fusion proteins were only expressed with pCDNA3.1. The BRET[1] curve was obtained by fitting the data points to a non-linear regression equation assuming a single binding site using GraphPad Prism version 6.00 (San Diego, CA, USA).

Patch-clamp experiments of astrocytes

Three days before the experiment, dB-cAMP-differentiated astrocytes were trypsinized and seeded at a density of $1 - 3 \times 10^4$ cells onto 24-well plates containing a glass coverslip with supplemented DMEM and 250 µM dBcAMP. The glass coverslip was mounted on the stage of inverted microscopy equipped with phase-contrast optics and fluorescence illumination. Patch pipettes were pulled from borosilicate glass capillaries (Clark Electromedical, UK) in a Flaming/Brown micropipettepuller P-97 (Sutter instruments). The electrophysiological recordings were performed with a patch clamp amplifier (Axopatch 200B, Molecular Devices, Union City, CA). The electrodes had a resistance of 4–5 MΩ when filled with intracellular solution (in mM): 144 NMDG-Cl, 2 $MgCl_2$, 5 EGTA, 5 HEPES, 5 Glucose with pH 7.3 and 300 mOsm/kg.

To measure VRAC and ClC-2 currents, the extracellular solution contained (in mM): 144 NMDG-Cl, 2 $CaCl_2$, 2 $MgCl_2$, 5 HEPES, 5 glucose, with pH 7.3 and 300 mOsm/kg. For VRAC, hypotonic extracellular solution (−25%) was obtained by decreasing the NMDG-Cl concentration to 105 mM (220 mOsm/kg). For ClC-2, the depolarizing extracellular solution contained (in mM): 144 NaCl, 11 KCl, 1.3 $CaCl_2$, 0.4 $MgSO_2$, 1.2 KH_2PO_4, 25 HEPES-NaOH, 10 glucose, with pH 7.2 and 300 mOsm/kg. All the solution osmolarities were adjusted with sorbitol. An Ag/AgCl ground electrode mounted in a 3 M KCl agar bridge was used. Membrane currents were recorded in the whole-cell patch clamp configuration, filtered at 2 kHz, digitized at 10 kHz and acquired with pClamp 10 software (Molecular Devices). Data were analyzed with Clampfit 10 (Molecular Devices) and Prism 4 (GraphPad Software, Inc., La Jolla, CA). Whole-cell capacitance and series resistance were compensated with the amplifier circuitry. Series resistance was always kept below 10 MΩ and compensated at 70–80%. All recordings were performed at room temperature (22–23°C). Currents were evoked in 4 s pulses from −120 to +50 mV (Δ10 mV) to measure ClC-2 currents and from −80 to +80 mV (Δ20 mV) to measure VRAC currents. The holding potential was 0 mV.

Statistics

Statistical significance was assessed between two groups using the unpaired or paired Student's test as appropiate. For statistical analyses of multiple groups, one-way analysis of variance and multiple comparison's test (Dunnet) versus control groups were performed.

Supplementary Material

Supplementary Material is available at *HMG* online.

Acknowledgements

This study was supported by MICINN (SAF 2015-70377 and RTI2018-093493-B-I00 and ISCIII (ERARE) to RE. RE was awarded with Icrea Academia prizes (2009 and 2014). A.G. and M.C.S. work has been financed by 'Fondation pour la recherche médicale' (PLP20170939025p60 to A.G.; AJE20171039094 to M.C.S.) and the European Leukodystrophies Association (ELA International) Research Foundation (2019-010 C4A). V.N. was supported by Spanish Health Institute Carlos III Grant PI16/00267-R-FEDER and Generalitat de Catalunya grant SGR2017-191. V.N. and R.E. thanks CERCA Programme/Generalitat de Catalunya for IDIBELL support. It was also funded by European Union, Fondo Europeo de Desarrollo regional, Ministerio de Ciencia e Innovación and Instituto de Salud Carlos III of Spain FIS P17/00296 (XG), RETICS Oftared RD16/0008/0014 (XG), Generalitat de Catalunya 2017SGR737 (XG) and Maria de Maeztu MDM-2017-0729 to Institut de Neurociencies, Universitat de Barcelona.
We thank Thomas Jentsch for providing brains from *Glialcam* KO mice and two different GlialCAM antibodies. We thank Esther prat for managing the colonies of KO mice.

Conflict of Interest statement. None declared.

References

1. van der Knaap, M.S.S., Boor, I. and Estévez, R. (2012) Megalencephalic leukoencephalopathy with subcortical cysts: chronic white matter oedema due to a defect in brain ion and water homoeostasis. *Lancet Neurol.*, **11**, 973–985.
2. Hamilton, E.M.C., Tekturk, P., Cialdella, F. *et al.* (2018) Megalencephalic leukoencephalopathy with subcortical cysts. *Neurology*, **90**, e1395–e1403.
3. Leegwater, P.A., Yuan, B.Q., van der Steen, *J. et al.* (2001) Mutations of MLC1 (KIAA0027), encoding a putative membrane protein, cause megalencephalic leukoencephalopathy with subcortical cysts. *Am. J. Hum. Genet.*, **68**, 831–838.
4. López-Hernández, T., Ridder, M.C., Montolio, M. *et al.* (2011) Mutant GlialCAM causes megalencephalic leukoencephalopathy with subcortical cysts, benign familial macrocephaly, and macrocephaly with retardation and autism. *Am. J. Hum. Genet.*, **88**, 422–432.
5. Lopez-Hernandez, T., Sirisi, S., Capdevila-Nortes, X. *et al.* (2011) Molecular mechanisms of MLC1 and GLIALCAM mutations in megalencephalic leukoencephalopathy with subcortical cysts. *Hum. Mol. Genet.*, **20**, 3266–3277.
6. Bosch, A. and Estévez, R. (2021) Megalencephalic leukoencephalopathy: insights into pathophysiology and perspectives for therapy. *Front. Cell. Neurosci.*, **14**, 627887.
7. Capdevila-Nortes, X., López-Hernández, T., Apaja, P.M. *et al.* (2013) Insights into MLC pathogenesis: GlialCAM is an MLC1 chaperone required for proper activation of volume-regulated anion currents. *Hum. Mol. Genet.*, **22**, 4405–4416.

8. Ridder, M.C., Boor, I., Lodder, J.C. *et al.* (2011) Megalencephalic leucoencephalopathy with cysts: defect in chloride currents and cell volume regulation. *Brain*, **134**, 3342–3354.
9. Jeworutzki, E., López-Hernández, T., Capdevila-Nortes, X. *et al.* (2012) GlialCAM, a protein defective in a leukodystrophy, serves as a ClC-2 Cl - channel auxiliary subunit. *Neuron*, **73**, 951–961.
10. Hoegg-Beiler, M.B., Sirisi, S., Orozco, I.J. *et al.* (2014) Disrupting MLC1 and GlialCAM and ClC-2 interactions in leukodystrophy entails glial chloride channel dysfunction. *Nat. Commun.*, **5**, 3475.
11. Sugio, S., Tohyama, K., Oku, S. *et al.* (2017) Astrocyte-mediated infantile-onset leukoencephalopathy mouse model. *Glia*, **65**, 150–168.
12. Wu, M., Moh, M.C. and Schwarz, H. (2016) HepaCAM associates with connexin 43 and enhances its localization in cellular junctions. *Sci. Rep.*, **6**, 36218.
13. Lanciotti, A., Brignone, M.S., Belfiore, M. *et al.* (2020) Megalencephalic leukoencephalopathy with subcortical cysts disease-linked MLC1 protein favors gap-junction intercellular communication by regulating connexin 43 trafficking in astrocytes. *Cell*, **9**, 1425.
14. Lanciotti, A., Brignone, M.S., Visentin, S. *et al.* (2016) Megalencephalic leukoencephalopathy with subcortical cysts protein-1 regulates epidermal growth factor receptor signaling in astrocytes. *Hum. Mol. Genet.*, **25**, 1543–1558.
15. Elorza-Vidal, X., Sirisi, S., Gaitán-Peñas, H. *et al.* (2018) GlialCAM/MLC1 modulates LRRC8/VRAC currents in an indirect manner: implications for megalencephalic leukoencephalopathy. *Neurobiol. Dis.*, **119**, 88–99.
16. Hirabayashi, Y. and Kim, Y.J. (2020) Roles of GPRC5 family proteins: focusing on GPRC5B and lipid-mediated signalling. Roles of GPRC5 family proteins: focusing on GPRC5B and lipid-mediated signalling. *J. Biochem.*, **167**, 541–547.
17. Smith, N.J. (2015) Drug discovery opportunities at the endothelin B receptor-related orphan g protein-coupled receptors, GPR37 and GPR37L1. Drug discovery opportunities at the endothelin B receptor-related orphan g protein-coupled receptors, GPR37 and GPR37L1. *Front. Pharmacol.*, **6**, 275.
18. Brignone, M.S., Lanciotti, A., Macioce, P. *et al.* (2011) The beta1 subunit of the Na,K-ATPase pump interacts with megalencephalic leucoencephalopathy with subcortical cysts protein 1 (MLC1) in brain astrocytes: new insights into MLC pathogenesis. *Hum. Mol. Genet.*, **20**, 90–103.
19. Meyer, R.C., Giddens, M.M., Schaefer, S.A. *et al.* (2013) GPR37 and GPR37L1 are receptors for the neuroprotective and glioprotective factors prosaptide and prosaposin. *Proc. Natl. Acad. Sci. U. S. A.*, **110**, 9529–9534.
20. Duarri, A., Lopez de Heredia, M., Capdevila-Nortes, X. *et al.* (2011) Knockdown of MLC1 in primary astrocytes causes cell vacuolation: a MLC disease cell model. *Neurobiol. Dis.*, **43**, 228–238.
21. Yang, H.J., Vainshtein, A., Maik-Rachline, G. *et al.* (2016) G protein-coupled receptor 37 is a negative regulator of oligodendrocyte differentiation and myelination. *Nat. Commun.*, **7**, 10884.
22. Marazziti, D., Di Pietro, C., Golini, E. *et al.* (2013) Precocious cerebellum development and improved motor functions in mice lacking the astrocyte cilium-, patched 1-associated Gpr37l1 receptor. *Proc. Natl. Acad. Sci. U. S. A.*, **110**, 16486–16491.
23. Sirisi, S., Elorza-Vidal, X., Arnedo, T. *et al.* (2017) Depolarization causes the formation of a ternary complex between GlialCAM, MLC1 and ClC-2 in astrocytes: implications in megalencephalic leukoencephalopathy. *Hum. Mol. Genet.*, **26**, 2436–2450.
24. Boulay, A.C., Saubaméa, B., Declèves, X. *et al.* (2015) Purification of mouse brain vessels. *J. Vis. Exp.*, (105), e53208.
25. Jolly, S., Bazargani, N., Quiroga, A.C. *et al.* (2018) G protein-coupled receptor 37-like 1 modulates astrocyte glutamate transporters and neuronal NMDA receptors and is neuroprotective in ischemia. *Glia*, **66**, 47–61.
26. Qiu, Z., Dubin, A.E., Mathur, J. *et al.* (2014) SWELL1, a plasma membrane protein, is an essential component of volume-regulated Anion Channel. *Cell*, **157**, 447–458.
27. Voss, F.K., Ullrich, F., Münch, J. *et al.* (2014) Identification of LRRC8 heteromers as an essential component of the volume-regulated anion channel VRAC. *Science*, **344**, 634–638.
28. Gaitán-Peñas, H., Apaja, P.M., Arnedo, T. *et al.* (2017) Leukoencephalopathy-causing CLCN2 mutations are associated with impaired Cl− channel function and trafficking. *J. Physiol.*, **595**, 6993–7008.
29. Sano, T., Kim, Y.J., Oshima, E. *et al.* (2011) Comparative characterization of GPRC5B and GPRC5C LacZ knockin mice; behavioral abnormalities in GPRC5B-deficient mice. *Biochem. Biophys. Res. Commun.*, **412**, 460–465.
30. Sano, T., Kohyama-Koganeya, A., Kinoshita, M.O. *et al.* (2018) Loss of GPRC5B impairs synapse formation of Purkinje cells with cerebellar nuclear neurons and disrupts cerebellar synaptic plasticity and motor learning. *Neurosci. Res.*, **136**, 33–47.
31. Sirisi, S., Folgueira, M., López-Hernández, T. *et al.* (2014) Megalencephalic leukoencephalopathy with subcortical cysts protein 1 regulates glial surface localization of GLIALCAM from fish to humans. *Hum. Mol. Genet.*, **23**, 5069–5086.
32. Larsen, B.R., Assentoft, M., Cotrina, M.L. *et al.* (2014) Contributions of the Na+/K+-ATPase, NKCC1, and Kir4.1 to hippocampal K+ clearance and volume responses. *Glia*, **62**, 608–622.
33. Larsen, B.R., Stoica, A. and MacAulay, N. (2016) Managing brain extracellular K+ during neuronal activity: the physiological role of the Na+/K+-ATPase subunit isoforms. Managing brain extracellular K+ during neuronal activity: the physiological role of the Na+/K+-ATPase subunit isoforms. *Front. Physiol.*, **7**, 141.
34. Djukic, B., Casper, K.B., Philpot, B.D. *et al.* (2007) Conditional knock-out of Kir4.1 leads to glial membrane depolarization, inhibition of potassium and glutamate uptake, and enhanced short-term synaptic potentiation. *J. Neurosci.*, **27**, 11354–11365.
35. Rouach, N., Koulakoff, A. and Giaume, C. (2004) Neurons set the tone of gap junctional communication in astrocytic networks. *Neurochem. Int.*, **45**, 265–272.
36. Pannasch, U., Vargova, L., Reingruber, J. *et al.* (2011) Astroglial networks scale synaptic activity and plasticity. *Proc. Natl. Acad. Sci.*, **108**, 8467–8472.
37. Bellot-Saez, A., Kékesi, O., Morley, J.W. *et al.* (2017) Astrocytic modulation of neuronal excitability through K+ spatial buffering. *Neurosci. Biobehav. Rev.*, **77**, 87–97.
38. Kofuji, P. and Newman, E.A. (2004) Potassium buffering in the central nervous system. *Neuroscience*, **129**, 1043–1054.
39. MacAulay, N. (2020) Molecular mechanisms of K+ clearance and extracellular space shrinkage—glia cells as the stars. Molecular mechanisms of K+ clearance and extracellular space shrinkage—glia cells as the stars. *Glia*, **68**, 2192–2211.

40. Theparambil, S.M., Hosford, P.S., Ruminot, I. *et al.* (2020) Astrocytes regulate brain extracellular pH via a neuronal activity-dependent bicarbonate shuttle. *Nat. Commun.*, **11**, 5073.
41. Charrin, S., Jouannet, S., Boucheix, C. *et al.* (2014) Tetraspanins at a glance. *J. Cell Sci.*, **127**, 3641–3648.
42. Ito, Y., Honda, A. and Igarashi, M. (2018) Glycoprotein M6a as a signaling transducer in neuronal lipid rafts. *Neurosci. Res.*, **128**, 19–24.
43. Zhang, X., Xie, H., Chang, P. *et al.* (2019) Glycoprotein M6B interacts with TβRI to activate TGF-β-Smad2/3 signaling and promote smooth muscle cell differentiation. *Stem Cells*, **37**, 190–201.
44. Zeng, Z., Su, K., Kyaw, H. *et al.* (1997) A novel endothelin receptor type-B-like gene enriched in the brain. *Biochem. Biophys. Res. Commun.*, **233**, 559–567.
45. Marazziti, D., Golini, E., Gallo, A. *et al.* (1997) Cloning of GPR37, a gene located on chromosome 7 encoding a putative g- protein-coupled peptide receptor, from a human frontal brain EST library. *Genomics*, **45**, 68–77.
46. Marazziti, D., Gallo, A., Golini, E. *et al.* (1998) Molecular cloning and chromosomal localization of the mouse Gpr37 gene encoding an orphan G-protein-coupled peptide receptor expressed in brain and testis. *Genomics*, **53**, 315–324.
47. Valdenaire, O., Giller, T., Breu, V. *et al.* (1998) A new family of orphan G protein-coupled receptors predominantly expressed in the brain. *FEBS Lett.*, **424**, 193–196.
48. Liu, B., Mosienko, V., Vaccari Cardoso, B. *et al.* (2018) Glio- and neuro-protection by prosaposin is mediated by orphan G-protein coupled receptors GPR37L1 and GPR37. *Glia*, **66**, 2414–2426.
49. Lundius, E.G., Vukojevic, V., Hertz, E. *et al.* (2014) GPR37 protein trafficking to the plasma membrane regulated by prosaposin and GM1 gangliosides promotes cell viability. *J. Biol. Chem.*, **289**, 4660–4673.
50. Meyer, R.C., Giddens, M.M., Coleman, B.M. *et al.* (2014) The protective role of prosaposin and its receptors in the nervous system. The protective role of prosaposin and its receptors in the nervous system. *Brain Res.*, **1585**, 1–12.
51. La Sala, G., Di Pietro, C., Matteoni, R. *et al.* (2020) Gpr37l1/prosaposin receptor regulates Ptch1 trafficking, Shh production, and cell proliferation in cerebellar primary astrocytes. *J. Neurosci. Res.*. doi: 10.1002/jnr.24775.
52. Kwon, S.H., Liu, K.D. and Mostov, K.E. (2014) Intercellular transfer of GPRC5B via exosomes drives HGF-mediated outward growth. *Curr. Biol.*, **24**, 199–204.
53. Kim, Y.J., Sano, T., Nabetani, T. *et al.* (2012) GPRC5B activates obesity-associated inflammatory signaling in adipocytes. *Sci. Signal.*, **5**, ra85.
54. Zambrano, S., Möller-Hackbarth, K., Li, X. *et al.* (2019) GPRC5B modulates inflammatory response in glomerular diseases via NF-κB pathway. *J. Am. Soc. Nephrol.*, **30**, 1573–1586.
55. von Samson-Himmelstjerna, F.A., Freundt, G., Nitz, J.T. *et al.* (2019) The orphan receptor GPRC5B modulates inflammatory and fibrotic pathways in cardiac fibroblasts and mice hearts. *Biochem. Biophys. Res. Commun.*, **514**, 1198–1203.
56. Kim, Y.J. and Hirabayashi, Y. (2018) Caveolin-1 prevents palmitate-induced NF-κB signaling by inhibiting GPRC5B-phosphorylation. *Biochem. Biophys. Res. Commun.*, **503**, 2673–2677.
57. Kim, Y.-J., Greimel, P. and Hirabayashi, Y. (2018) GPRC5B-mediated sphingomyelin synthase 2 phosphorylation plays a critical role in insulin resistance. *iScience*, **8**, 250–266.
58. Brignone, M.S., Lanciotti, A., Serafini, B. *et al.* (2019) Megalencephalic leukoencephalopathy with subcortical cysts Protein-1 (MLC1) counteracts astrocyte activation in response to inflammatory signals. *Mol. Neurobiol.*, **56**, 8237–8254.
59. Hemler, M.E. (2005) Tetraspanin functions and associated microdomains. Tetraspanin functions and associated microdomains. *Nat. Rev. Mol. Cell Biol.*, **6**, 801–811.
60. Robert, J.M.H., Amoussou, N.G., Le Mai, H. *et al.* (2021) Tetraspanins: useful multifunction proteins for the possible design and development of small-molecule therapeutic tools. Tetraspanins: useful multifunction proteins for the possible design and development of small-molecule therapeutic tools. *Drug Discov. Today*, **26**, 56–68.
61. Susa, K.J., Rawson, S., Kruse, A.C. *et al.* (2021) Cryo-EM structure of the B cell co-receptor CD19 bound to the tetraspanin CD81. *Science*, **371**, 300–305.
62. Oosterheert, W., Xenak, K.T., Neviani, V. *et al.* (2020) Implications for tetraspanin-enriched microdomain assembly based on structures of CD9 with EWI-F. *Life Sci. Alliance*, **3**, e202000883.
63. Barreiro, O., Zamai, M., Yáñez-Mó, M. *et al.* (2008) Endothelial adhesion receptors are recruited to adherent leukocytes by inclusion in preformed tetraspanin nanoplatforms. *J. Cell Biol.*, **183**, 527–542.
64. Little, K.D., Hemler, M.E. and Stipp, C.S. (2004) Dynamic regulation of a GPCR-Tetraspanin-G protein complex on intact cells: central role of CD81 in facilitating GPR56-Gαq/11 association. *Mol. Biol. Cell*, **15**, 2375–2387.
65. Termini, C.M. and Gillette, J.M. (2017) Tetraspanins function as regulators of cellular signaling. Tetraspanins function as regulators of cellular signaling. *Front. Cell Dev. Biol.*, **5**, 34.
66. Yang, Y., Liu, X.R., Greenberg, Z.J. *et al.* (2020) Open conformation of tetraspanins shapes interaction partner networks on cell membranes. *EMBO J.*, **39**, e105246.
67. Schwenk, J., Harmel, N., Brechet, A. *et al.* (2012) High-resolution proteomics unravel architecture and molecular diversity of native AMPA receptor complexes. *Neuron*, **74**, 621–633.
68. Bildl, W., Haupt, A., Müller, C.S. *et al.* (2012) Extending the dynamic range of label-free mass spectrometric quantification of affinity purifications. *Mol. Cell. Proteomics*, **11**, M111.007955.
69. Sokolina, K., Kittanakom, S., Snider, J. *et al.* (2017) Systematic protein–protein interaction mapping for clinically relevant human GPCRs. *Mol. Syst. Biol.*, **13**, 918.
70. La Sala, G., Marazziti, D., Di Pietro, C. *et al.* (2015) Modulation of Dhh signaling and altered Sertoli cell function in mice lacking the GPR37-prosaposin receptor. *FASEB J.*, **29**, 2059–2069.
71. Teijido, O., Martinez, A., Pusch, M. *et al.* (2004) Localization and functional analyses of the MLC1 protein involved in megalencephalic leukoencephalopathy with subcortical cysts. *Hum. Mol. Genet.*, **13**, 2581–2594.
72. Di Pietro, C., La Sala, G., Matteoni, R. *et al.* (2019) Genetic ablation of Gpr37l1 delays tumor occurrence in Ptch1 +/− mouse models of medulloblastoma. *Exp. Neurol.*, **312**, 33–42.
73. Ferroni, S., Marchini, C., Nobile, M. *et al.* (1997) Characterization of an inwardly rectifying chloride conductance expressed by cultured rat cortical astrocytes. *Glia*, **21**, 217–227.
74. Schneider, C.A., Rasband, W.S. and Eliceiri, K.W. (2012) NIH image to ImageJ: 25 years of image analysis. *Nat. Methods*, **9**, 671–675.